MOLECULAR AND CELLULAR BIOLOGY, Aug. 2010, p. 3994–4005 Vol. 30, No. 16
0270-7306/10/$12.00 doi:10.1128/MCB.01358-09

The Anaphase-Promoting Complex/Cyclosome Activator Cdh1 Modulates Rho GTPase by Targeting p190 RhoGAP for Degradation▽†

Hideaki Naoe,[1,4] Kimi Araki,[3] Osamu Nagano,[1,2] Yusuke Kobayashi,[1] Jo Ishizawa,[1] Tatsuyuki Chiyoda,[1] Takatsune Shimizu,[1,2] Ken-ichi Yamamura,[3] Yutaka Sasaki,[4] Hideyuki Saya,[1,2] and Shinji Kuninaka[1]*

Division of Gene Regulation, Institute for Advanced Medical Research, Keio University School of Medicine, Tokyo 160-8582, Japan[1]; CREST, Japan Science and Technology Agency, Tokyo 102-0075, Japan[2]; and Laboratory of Developmental Genetics, Division of Organogenesis, Institute of Molecular Embryology and Genetics,[3] and Department of Gastroenterology and Hepatology, School of Medicine,[4] Kumamoto University, Kumamoto 860-8556, Japan

Received 12 October 2009/Returned for modification 30 November 2009/Accepted 24 May 2010

Cdh1 is an activator of the anaphase-promoting complex/cyclosome and contributes to mitotic exit and G_1 maintenance by targeting cell cycle proteins for degradation. However, Cdh1 is expressed and active in postmitotic or quiescent cells, suggesting that it has functions other than cell cycle control. Here, we found that homozygous *Cdh1* gene-trapped (*Cdh1*$^{GT/GT}$) mouse embryonic fibroblasts (MEFs) and *Cdh1*-depleted HeLa cells reduced stress fiber formation significantly. The GTP-bound active Rho protein was apparently decreased in the *Cdh1*-depleted cells. The p190 protein, a major GTPase-activating protein for Rho, accumulated both in *Cdh1*$^{GT/GT}$ MEFs and in *Cdh1*-knockdown HeLa cells. Cdh1 formed a physical complex with p190 and stimulated the efficient ubiquitination of p190, both in *in vitro* and *in vivo*. The motility of *Cdh1*-depleted HeLa cells was impaired; however, codepletion of p190 rescued the migration activity of these cells. Moreover, *Cdh1*$^{GT/GT}$ embryos exhibited phenotypes similar to those observed for Rho-associated kinase I and II knockout mice: eyelid closure delay and disruptive architecture with frequent thrombus formation in the placental labyrinth layer, respectively. Furthermore, the p190 protein accumulated in the *Cdh1*$^{GT/GT}$ embryonic tissues. Our data revealed a novel function for Cdh1 as a regulator of Rho and provided insights into the role of Cdh1 in cell cytoskeleton organization and cell motility.

The anaphase-promoting complex/cyclosome (APC/C) is a multisubunit complex that functions as an E3 ubiquitin ligase for various cell cycle proteins (19, 46). Proteins ubiquitinated by APC/C are recognized and degraded by the 26S proteasome to ensure proper cell cycle progression. APC/C activity is strictly dependent on coactivator proteins that interact with APC/C during specific phases of the cell cycle. Cdh1 (also known as Fzr, Hct1, or Srw) is one of the coactivators that maintain APC/C activity from anaphase of mitosis until the end of the G_1 phase of the cell cycle (43, 53).

The role of Cdh1 (APC/C^{Cdh1}) on cell-cycle progression has been well studied; however, several studies have shed light into another aspect of Cdh1's function. For example, expression of Cdh1 is not restricted to cycling cells; APC/C^{Cdh1} is also present and active in quiescent cultured cells (9). Furthermore, immunohistochemical analysis has shown that Cdh1 is expressed in a wide variety of tissues that are predominantly composed of postmitotic cells, such as neurons, where APC/C^{Cdh1} has a high cyclin B ubiquitination activity (1, 16). It has been reported that APC/C^{Cdh1} promotes axonal growth and patterning (20) and is required for neuronal survival (1). These results highlight the importance of the APC/C activator Cdh1 in neurons. However, Cdh1 has also been shown to participate in the differentiation of tissues such as the muscle (25). Given that Cdh1 is ubiquitously expressed in organs containing quiescent cells, there might be additional roles for Cdh1.

Rho GTPase proteins play a central role in the regulation of cell shape, polarity, and locomotion via their effects on actin polymerization, actomyosin contractility, cell adhesion, and microtubule dynamics (13). Small G proteins, which include Rho, act as molecular switches that cycle between an inactive GDP-bound state and an active GTP-bound state. The latter form of Rho proteins interacts with and activates downstream effector proteins. The activity of Rho GTPases is controlled by three class of key regulators: (i) guanine nucleotide exchange factors (GEFs), which catalyze the exchange of GDP to GTP for their activation (41); (ii) GTPase activating proteins (GAPs), which stimulate the intrinsic GTPase activity for their inactivation (8); and (iii) guanine nucleotide dissociation inhibitors (GDIs), which interact with GDP-bound Rho GTPases and sequester them in the cytoplasm to inhibit the exchange of GDP to GTP (33). In addition to these canonical regulations, recent studies indicate that the ubiquitination pathway is also involved in the modulation of Rho GTPase activity. Smurf1, which is a HECT domain E3 ubiquitin ligase, controls the local levels of RhoA at the cell periphery by targeting it for degradation (40, 55). Therefore, the regulatory mechanisms of Rho GTPase activity seem to be more complex than previously thought. It thus remains to be clarified whether

* Corresponding author. Mailing address: Division of Gene Regulation, Institute for Advanced Medical Research, Keio University School of Medicine, Tokyo 160-8582, Japan. Phone: 81 3 5363 3983. Fax: 81 3 5363 3982. E-mail: skuninak@a8.keio.jp.

† Supplemental material for this article may be found at http://mcb.asm.org/.

▽ Published ahead of print on 7 June 2010.

other ubiquitin ligases also play a role in Rho signaling by targeting its components directly or indirectly.

In this study, we found that the APC/C activator Cdh1 modulated actin organization. Mouse embryonic fibroblasts (MEFs) derived from a homozygous *Cdh1* gene-trapped ([GT] $Cdh1^{GT/GT}$) mouse model displayed decreased numbers of stress fibers and focal adhesions (FAs). Consistent with these phenotypes, Rho activity was apparently reduced in *Cdh1*-deficient cells. Cdh1 regulated Rho activity via the targeting of p190 for degradation. We also found that Cdh1 knockdown cells showed decreased motility, which was rescued by codepletion of p190. Furthermore, phenotypic similarities between $Cdh1^{GT/GT}$ embryos and ROCK (also known as Rho-kinase, which is the important Rho downstream effector of actin cytoskeleton formation) knockout (KO) mice (44, 49) support our notion that Cdh1 plays a role in the Rho/ROCK signaling axis. Collectively, our findings suggest an alternative role for Cdh1 other than cell cycle regulation and reveal Cdh1 as a new regulator of Rho.

MATERIALS AND METHODS

Mice. $Cdh1^{+/GT}$ mice (C57BL/6 background) were derived from the TT2 embryonic stem (ES) cell line (57) by integration of the pU-17 exchangeable GT vector (48) into the *Cdh1* locus. These mice were obtained from TransGenic (Kumamoto, Japan). Characterization of the vector insertion site was performed by 5′ rapid amplification of cDNA ends (5′ RACE) and plasmid rescue experiments. Genotyping of the mutant mice was performed using a PCR protocol based on the primers Gs4 (5′-CCTCCACTACAGCAGCACG-3′), Gas7 (5′-CTCCAAGGCCTTTGTGAGGC-3′), and SA6as (5′-CCGGCTAAAACTTGAGACCTTC-3′) (see Fig. S1 in the supplemental material). For detection of the Cdh1–β-*geo* fusion mRNA, oligo(dT)-primed cDNAs derived from mutant mice were subjected to PCR using the primers 5NC-s (5′-TGTTCCTGGGACCGGCGGGAAC-3′) and LZUS-3 (5′-CGCATCGTAACCGTGCATCT-3′). The amplification product was cloned into the TA cloning vector and sequenced. All animal experiments were approved by the Animal Ethics Committees of Keio University and Kumamoto University.

Replacement of the β-*geo* gene cassette. To produce ES cells in which the β-*geo* gene cassette of $Cdh1^{+/GT}$ cells was replaced with the *Cdh1* cDNA, we introduced the P17/Cdh1 replacement vector (see Fig. S2C in the supplemental material) together with pCAGGS-Cre (encoding Cre recombinase) (3) into $Cdh1^{+/GT}$ ES cells using electroporation. Cells were cultured in medium containing puromycin for 1 day to isolate cell lines that had undergone recombination. Puromycin selection was performed twice at a 2-day interval. To detect the expression of the knock-in (KI) *Cdh1* ($Cdh1^{KI}$) allele, we performed reverse transcription-PCR (RT-PCR) analysis using the primers 5NC-s2 (5′-TCGAACAGGCGCGGCGTGTT-3′) and mFzr as2 (5′-ATAGTCCTGGTCCATGGTGGAG-3′) (see Fig. S2C). The PCR product was cloned into the pGEM-T easy vector (Promega) and sequenced.

Cell culture and transfection. MEFs were prepared as follows. After mating with $Cdh1^{+/GT}$ male mice, a pregnant female $Cdh1^{+/GT}$ mouse was sacrificed at 11.5 days postcoitus (dpc), and the uterus was removed and washed in phosphate-buffered saline (PBS). The yolk sacs were separated for genotyping, and the embryos were isolated and washed in PBS. The viscera of each embryo were removed under a dissecting microscope, and the embryo was washed in PBS and incubated with TrypLE Express (Invitrogen) for 20 min at 37°C. The cell suspension was then passed several times through a pipette and filtered through a sterile cell strainer (100-μm pore size) to remove cell clumps. The cell suspension prepared from each embryo was washed with medium containing 10% fetal bovine serum (FBS) and plated onto 100-mm culture dishes. MEFs were maintained in Dulbecco's modified Eagle's medium (DMEM)-F12 supplemented with 10% FBS and antibiotics. For immortalization of MEFs, primary MEFs were transfected with simian virus 40 (SV40) large T antigen, which was prepared by transfection of Plat-E cells with pWZL-hyg-SV40 large T (28). Cells were selected in medium containing hygromycin for a week. The resultant immortalized MEFs were maintained in the medium described above. The human embryonic kidney cell line HEK293T (RCB2202) was provided by the RIKEN BRC through the National Bio-Resource Project of the MEXT, Japan. Culture and transfection of HeLa and HEK293T cells were performed as described previously (23). pEGFP-c/full-length p190 (where EGFP is enhanced green fluorescent protein) was kindly provided by H. Sabe (51). Cells were subjected to transient transfection in six-well plates using Fugene HD reagent (Roche). The transfection procedures used in the RNA interference (RNAi) experiments and the small interfering RNA (siRNA) oligonucleotides for Cdh1 and the control were as described previously (23). The target sequences of other siRNAs were as follows: siEmi1, 5′-GAGAAUUUCGGUGACAGUCUA-3′ (27), and sip190, 5′-UUGACAUCGUGGAAGUGAAGA-3′.

Quantitative analysis of gene expression. Total RNA was extracted from MEFs using an RNeasy Minikit (Qiagen) and was subjected to RT using PrimeScript (Takara). Real-time PCR was performed in a Thermal Cycler Dice (Takara) using SYBR Premix Ex *Taq* (Takara). The primers used for the amplification of murine *p190* and the glyceraldehyde-3-phosphate dehydrogenase gene (*GAPDH*) were obtained from Takara. Relative mRNA levels were calculated by normalization of the cycle threshold (C_T) values of the target gene to those of the reference gene (*GAPDH*).

Immunofluorescence microscopy. MEFs or HeLa cells were seeded onto 35-mm dishes (5×10^4 cells per dish) the day before the analysis. Cells were fixed with 4% paraformaldehyde-PBS for 15 min, which was followed by permeabilization with 0.2% Triton X-100–PBS. Cells were then incubated and stained with an antipaxillin antibody. This was followed by incubation with Alexa Fluor 488-conjugated phalloidin and Alexa Fluor 555-conjugated anti-mouse antibody (Molecular Probes). The stained cells were mounted with 1,4-diazabicyclo-[2,2,2]-octane–glycerol and were examined using a confocal microscope (FV300; Olympus). Densitometric analysis of the signal of each cell labeled with Alexa Fluor 488-conjugated phalloidin was performed using MetaXpress software (Molecular Devices).

Histochemistry, immunostaining, and X-Gal (5-bromo-4-chloro-3-indolyl-β-D-galactopyranoside) staining. For histological analysis, tissues were fixed overnight with 4% paraformaldehyde in PBS, embedded in paraffin, and then sectioned and stained with hematoxylin-eosin. For immunochemistry of eyelid epithelial sheets, 4-μm sections were prepared from 18.5-dpc embryos and boiled for 20 min in citrate buffer (pH 7.0) in a microwave oven to retrieve antigens. Nonspecific sites were blocked with mouse-on-mouse (MOM; Vector Laboratories) solution in PBS for 1 h. Sections were incubated overnight with mouse anti-p190 (1:50; BD) in MOM diluent, washed three times with PBS, and incubated with biotinylated anti-mouse IgG in MOM diluent for 10 min. Staining and development were performed using Elite ABC reagent (Vector Laboratories) and diaminobenzidine (DAB) substrate (Wako). For immunostaining of whole embryos, 12.5-dpc embryos were embedded in Tissue-Tek OCT compound medium (Sakura) and frozen in acetone-dry ice. Cryosections were stained as described above.

Immunoprecipitation, Western blotting, and antibodies. Immunoprecipitation and Western blotting were performed as described previously (23) with slight modification. We used magnetic Dynal beads (Invitrogen) for immunoprecipitation instead of agarose beads. The antibodies used in this study were anti-Myc (9E10; Santa Cruz Biotechnology), 1:1,000; anti-HA (12CA5; Santa Cruz Biotechnology), 1:1,000; anti-GFP (full-length; Santa Cruz Biotechnology), 1:500; anti-Cdh1 (DH01; Abcam), 1:500; anti-p190 (BD), 1:1,000; anti-α-tubulin (B-5-1-2; Sigma), 1:50,000; anti-RhoA, -B, and -C (Cell Signaling), 1:1,000; anti-Rac1 (Upstate Biotechnology), 1:1,000; anti-RhoGDI (Millipore), 1:500; anti-Skp2 (Zymed), 1:250; anti-cyclin B (GNS1; Santa Cruz), 1:200; and anti-Emi1 (Zymed), 1:200; anti-cdc27 (AF3.1; Santa Cruz Biotechnology), 1:500; and anti-His (MBL), 1:500. For immunoprecipitation and Western blotting of Cdh1, we generated a polyclonal antibody against Cdh1 by injecting rabbits with a synthetic peptide (MDQDYERRLLRQII, corresponding to mouse Cdh1 amino acids 1 to 14) coupled to keyhole limpet-hemocyanin (KLH) via a cysteine added at the C terminus.

Rho activation assay. HEK293 cells were transfected with siRNA oligonucleotides against Cdh1 or control. After 48 h of transfection, cells were treated with lysophosphatidic acid ([LPA] 10 μM; Sigma) for 10 min before being harvested. Cells were lysed by incubation with magnesium-containing buffer (25 mM HEPES, pH 7.5, 150 mM NaCl, 1% Igepal CA-630, 10 mM $MgCl_2$, 1 mM EDTA, and 2% glycerol) supplemented with 25 mM sodium fluoride, 1 mM sodium orthovanadate, 20 μM MG132, and protease inhibitor cocktail (Roche). After centrifugation of the lysate at 14,000 × *g* for 5 min at 4°C, the resulting supernatant was incubated with 25 μg of glutathione *S*-transferase (GST)-RBD (where RBD is the Rho-binding domain of rhotekin [amino acids 7 to 89]) bound to glutathione-Sepharose beads (GE Health Care) for 30 min at 4°C. The beads were then washed three times with magnesium-containing buffer and were subjected to immunoblot analysis using an anti-RhoA, -B, and -C polyclonal antibodies (Upstate Biotechnology). Whole-cell lysates were also immunoblotted for Rho as a loading control.

***In vitro* and *in vivo* ubiquitination assays.** For production of recombinant Cdh1 protein, a mouse Cdh1 cDNA was subcloned into pFASTBAC1 (Invitrogen) with an oligonucleotide linker corresponding to a penta-His tag. Baculoviruses were prepared according to the manufacturer's instructions (Invitrogen). Sf9 cells were transfected at a multiplicity of infection (MOI) of 10 with baculovirus for 72 h. Recombinant Cdh1 proteins were purified using a Ni-nitrilotriacetic acid (NTA) spin kit (Qiagen). The *in vitro* ubiquitination assay was performed as described previously (22, 47) with slight modification. Briefly, HeLa cells were lysed in lysis buffer (0.5% NP-40, 25 mM Tris-Cl [pH 7.5], 150 mM NaCl, 1 mM $MgCl_2$, 10% glycerol, and complete protease inhibitor cocktail [EDTA free; Roche]). APC/C was immunoprecipitated from the lysates using an anti-cdc27 antibody (Santa Cruz Biotechnology). Immunopurified APC/C was bound to recombinant Cdh1 protein and was then subjected to the ubiquitination reaction. APC/C-bound antibody beads were mixed with a reaction buffer (20 mM Tri-Cl [ph7.5], 150 mM NaCl, 1 mM dithiothreitol [DTT], 10% glycerol) containing purified E1 (80 μg/ml; Biomol), UbcH10 and UbcH5a (50 μg/ml each; Wako), ubiquitin (1.25 mg/ml; Sigma), ATP regenerating system (10 mM creatine phosphate, 2 mM ATP, 1 mM $MgCl_2$, 0.1 mM EGTA, and 39 U/ml rabbit creatine phosphokinase type I), and substrate (22). Myc-tagged full-length p190 protein (which was used as a substrate) was generated by *in vitro* translation using a TNT T7 Quick Coupled Transcription/Translation System (Promega) and biotinylated lysine (Promega Transcend tRNA), according to the manufacturer's instructions. Ubiquitinated p190 was detected by using anti-p190 antibody or streptavidin-horseradish peroxidase ([HRP] Promega). For *in vivo* ubiquitination assays, 293T cells transfected with a plasmid encoding hemagglutinin (HA)-tagged human ubiquitin and pEGFP-c/full-length p190 were incubated with 10 μM MG132 for 6 h after 24 h of cell culture. Cells were collected and subjected to immunoprecipitation using an anti-GFP antibody. Samples were immunoblotted to detect polyubiquitination using an anti-HA antibody.

Cell migration assay. Cell migration was measured using a 24-well Boyden chamber (BD). HeLa cells were transfected with siRNA 48 h before the assay. Cells (5×10^4) were seeded in serum-free medium (0.5 ml) in the upper chamber, with serum-containing medium in the lower chamber. After 24 h of incubation at 37°C, nonmigrating cells in the upper chamber were scraped using a cotton swab, and the undersides of the membranes were fixed with 100% methanol and stained with 50% Giemsa solution. The migrating cells at the bottom of the filters were counted (four fields per filter) in three independent experiments.

Establishment of *Cdh1*$^{GT/GT}$ ES cells and tetraploid aggregation experiments. To generate *Cdh1*$^{GT/GT}$ ES cell lines, we cultured delayed two-cell-stage embryos obtained by *in vitro* fertilization until the blastocyst stage and established ES cell lines as described previously (4, 31). The cell lines obtained were genotyped as described above. For tetraploid aggregation experiments, two-cell-stage embryos derived from crosses of BDF1 females with ICA;CAG-EGFP-IRES-puromycin males (in which the EGFP gene was ubiquitously expressed) were collected in KSOM medium (ARK Resource, Kumamoto, Japan). Embryos were then equilibrated in fusion buffer (0.3 M mannitol, 0.1 mM $MgSO_4$, polyvinyl alcohol [0.1 mg/ml], bovine serum albumin F-V [3 mg/ml; Sigma]) and placed between the electrodes of an electrofusion chamber (1-mm gap). Electrofusion was performed using a pulse generator (ECM2001; BTX, San Diego, CA) by application of two 40-μs pulses at 80 V/cm. Fused embryos were cultured in KSOM medium at 37°C for 40 h. *Cdh1*$^{GT/GT}$ or wild-type ES cells were then aggregated with the tetraploid embryos and transferred to pseudopregnant foster mothers (29, 31).

Scanning electron microscopy. The eyelids of embryos at 14.5 to 18.5 dpc were dissected under a stereoscopic microscope and fixed in 0.1 M sodium phosphate buffer (pH 7.4) containing 2% glutaraldehyde and 2% formaldehyde. Samples were washed and dehydrated in a graded series of ethanol, dried, sputter coated according to standard procedures, and then examined under a scanning electron microscope.

RESULTS

Effects of Cdh1 ablation on actin cytoskeleton organization. The role of Cdh1 has been investigated mainly as a regulator of the cell cycle using mammalian cultured cells or model organisms, such as flies and *Saccharomyces cerevisiae* (35). To further elucidate the physiological functions of Cdh1, we analyzed *Cdh1* gene-trapped (GT) mice generated using the exchangeable pU-17 GT vector, which encodes the β-galactosidase-neomycin resistance (β-*geo*) fusion gene (see Fig. S1 in the supplemental material). Homozygous *Cdh1* GT (*Cdh1*$^{GT/GT}$) mouse embryonic fibroblasts (MEFs) had a severely reduced abundance of Cdh1 expression, both at the RNA (less than 2% of that observed in wild-type MEFs) and protein levels (see Fig. S1). To investigate the role of Cdh1 on mammalian cellular behavior, we first analyzed asynchronously proliferating *Cdh1*$^{GT/GT}$ MEFs using time-lapse microscopy. We noticed a slight reduction in the cellular motility of *Cdh1*$^{GT/GT}$ MEFs compared with wild-type MEFs (data not shown). One possible reason for this difference could be proliferation defects in *Cdh1*$^{GT/GT}$ MEFs. To explore other possibilities, we focused on actin cytoskeletal architecture, which also plays an important role in cell motility. We compared the distribution of F-actin between *Cdh1*$^{GT/GT}$ MEFs and control cells (Fig. 1A). Immunofluorescence analysis of Alexa Fluor 488-conjugated phalloidin-labeled cells revealed that Cdh1 deficiency led to a striking phenotype that was characterized by fewer bundled actin stress fibers in the cell body and a more disorganized appearance (Fig. 1A, frames a and b). We quantified stress fiber density by incorporating a line profile across the cytoplasm that identified stress fibers by their increased fluorescence relative to areas devoid of stress fibers (Fig. 1B). Sharp, distinct peaks in fluorescence intensity within each line profile represented individual stress fibers crossed by the lines, as shown in Fig. 1B. Quantification of these peaks showed a significant decrease in Cdh1$^{GT/GT}$ MEFs compared with wild-type cells; however, the formation of cortical actin was preserved in Cdh1$^{GT/GT}$ MEFs (Fig. 1B). To further confirm the observation from MEFs, we transfected HeLa cells with an siRNA oligonucleotide against Cdh1 (Fig. 1C) and then analyzed the cytoskeletal architecture of these cells. *Cdh1*-deficient cells showed reduced stress fiber organization (Fig. 1C, frames a and b). The inhibitory effect of Cdh1 on actin stress fiber formation was enhanced under serum-free culture conditions (Fig. 1C, frames c and d). Moreover, we used the N-terminal fragment of Cdh1 (DN-Cdh1), which lacks the substrate-binding C terminus of Cdh1 and functions in a dominant negative fashion (54), to evaluate the role of Cdh1 in stress fiber formation. HeLa cells that expressed GFP–DN-Cdh1 tended to display a flattened shape, had reduced stress fibers, and exhibited reorganized cortical actin compared with surrounding nontransfected cells (Fig. 1D and E). The expression of DN-Cdh1 had the same effect on stress fibers in NIH 3T3 cells as in HeLa cells (Fig. 1F). These results suggest that Cdh1 played a regulatory role in the actin cytoskeleton of cells of different origins.

Focal adhesion remodeling usually accompanies actin rearrangements (42). We next examined whether actin fiber disassembly in *Cdh1*-deficient cells correlated with changes in FA formation. Immunostaining of paxillin, which is a major component of FAs, revealed that paxillin-labeled FAs were reduced in size and number, both in *Cdh1*$^{GT/GT}$ MEFs and in *Cdh1*-depleted HeLa cells (Fig. 1A, frames c and d, and C, frames e and f). We also observed that serum starvation reduced paxillin expression substantially in *Cdh1*-depleted cells (Fig. 1C, frames g and h). Collectively, our data suggest that Cdh1 played a role in the formation of FAs and stress fibers.

Cdh1 regulated Rho GTPase activity. Rho GTPases are important regulators of the actin cytoskeleton. To address the molecular mechanisms of stress fiber disassembly in

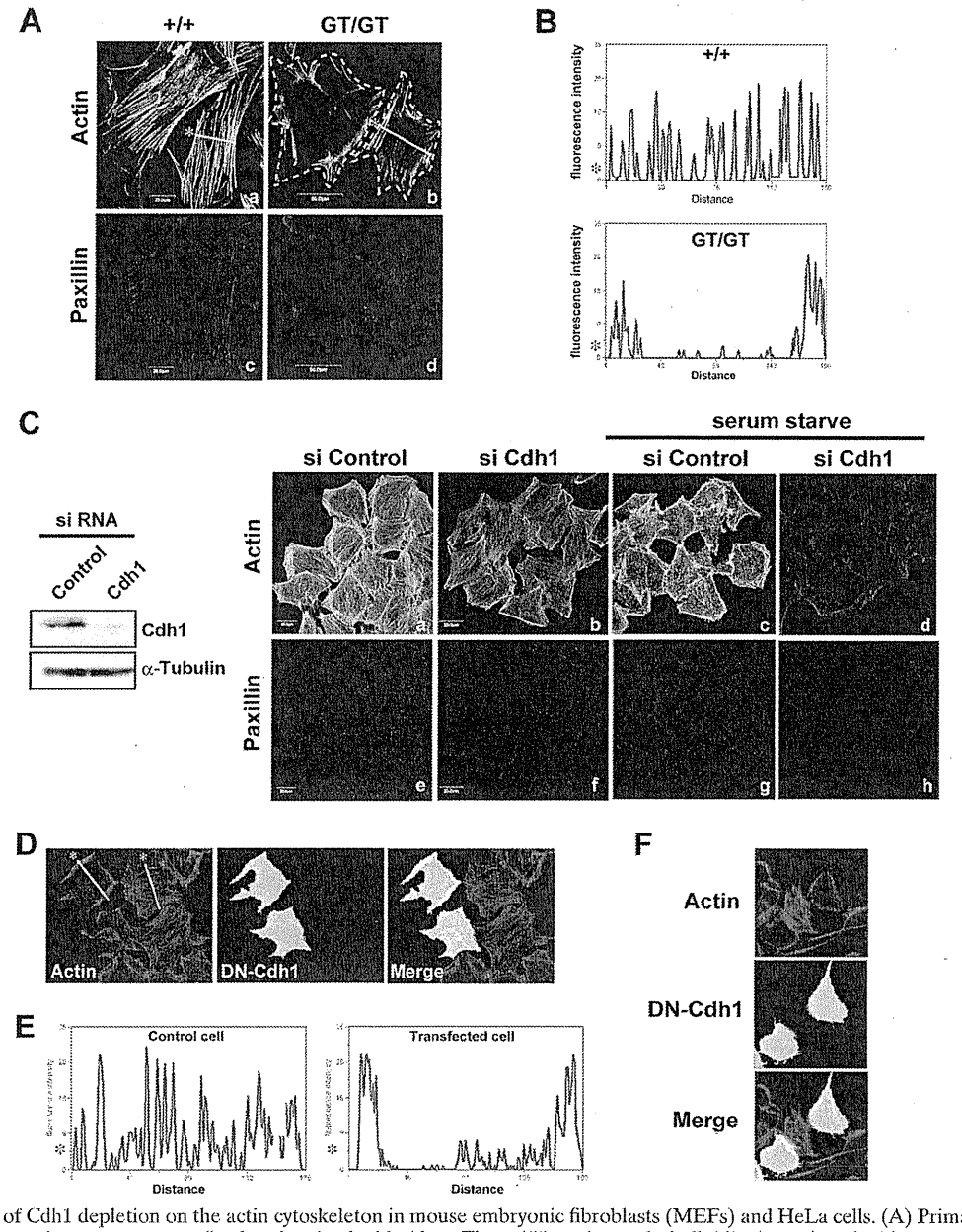

FIG. 1. Effects of Cdh1 depletion on the actin cytoskeleton in mouse embryonic fibroblasts (MEFs) and HeLa cells. (A) Primary MEFs derived from *Cdh1*$^{+/GT}$ mouse intercrosses were fixed and stained with Alexa Fluor 488-conjugated phalloidin (green) and with an antipaxillin antibody (red). The areas outlined by the dotted lines depict the cell bodies of *Cdh1*$^{GT/GT}$ MEFs. Bars, 20 μm (a and c) and 50 μm (b and d). (B) Quantification of fluorescent intensity across the yellow lines shown in the corresponding panels in A (to indicate stress fiber density) using the MetaXpress software (Molecular Devices). The asterisks denote the cells quantified in panel A and their corresponding line graphs B. (C) HeLa cells were transfected with a control siRNA oligonucleotide or with an siRNA oligonucleotide against Cdh1 and cultured for 2 days. The levels of expression of Cdh1 were evaluated using immunoblot analysis (left panels). HeLa cells transfected as described above were cultured in medium containing 10% serum (frames a, b, e, and f) or in serum-free medium (frames c, d, g, and h) for 24 h, fixed, and stained with Alexa Fluor 488-phalloidin (upper panels) and with an antipaxillin antibody (lower panels). Bars, 20 μm. (D) HeLa cells were transfected for 24 h with a GFP-tagged N-terminal fragment (residues 1 to 125) of Cdh1, which lacks the substrate-binding domain (WD-40 repeats) and acts in a dominant negative (DN) fashion (DN-Cdh1). Cells were then stained for rhodamine-phalloidin. (E) Quantification of fluorescence intensity across the yellow lines shown in panel D, as described for panel B. (F) NIH 3T3 cells were treated and analyzed as in panel D.

Cdh1$^{GT/GT}$ MEFs, we examined the abundance of Rho-family GTPases in these cells. We observed no significant differences in the protein expression levels of the Rho GTPases analyzed, with the exception of cdc42, which was not detected in MEFs (Fig. 2A). Thereafter, we focused on Rho because of its central role in the regulation of contractile actin-myosin stress fibers and of the assembly of FAs (38). RhoGDI has been shown to regulate Rho activity by binding GDP-bound RhoA (33). However, we found no changes in the levels of RhoGDI in *Cdh1*$^{GT/GT}$ MEFs (Fig. 2A), which excludes the possibility that

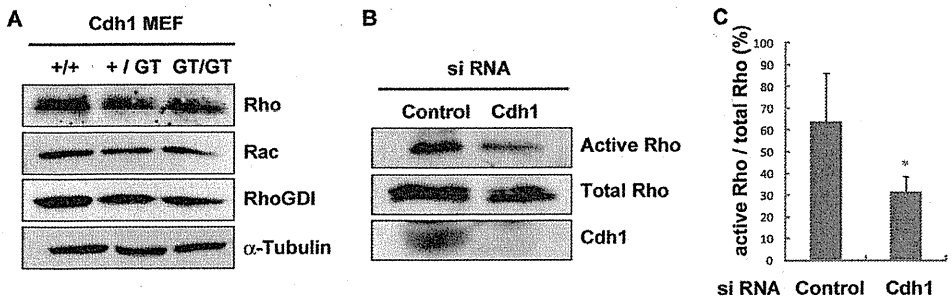

FIG. 2. Rho activity was decreased in *Cdh1*-depleted cells. (A) Cell lysates from wild-type or $Cdh1^{GT/GT}$ MEFs adjusted to equal protein concentrations were electrophoresed and transferred to nitrocellulose for immunoblot analysis using anti-Rho, anti-Rac, and anti-RhoGDI antibodies. α-Tubulin levels are shown as a loading control. (B) 293T cells were transfected with an siRNA directed against Cdh1 or with a control and were lysed after 2 days of cell culture. The GST-rhotekin RBD was incubated with the cell lysates to pull down active Rho. The levels of RBD-bound Rho and total Rho in cell lysates were determined by immunoblotting using an anti-Rho antibody. A representative result of three individual experiments is shown. (C) Quantification of the immunoblotting data in panel B was performed using densitometry. Data (arbitrary units) were normalized to the amount of total Rho and represent means ± standard deviations from three independent experiments (*, $P < 0.05$, Student's *t* test).

Cdh1 regulated Rho activity via the upregulation of its GDP-bound inactive form. We next analyzed Rho activity by affinity precipitation assay using a GST fusion protein containing the RhoA-binding domain of rhotekin (36, 37). 293T cells were stimulated with LPA for 10 min before harvesting, and the levels of bound active RhoA were measured. As shown in Fig. 2B, Cdh1 siRNA-transfected cells showed a marked decrease in GTP-bound Rho protein compared with control cells. Quantification of Rho activity revealed that Cdh1 depletion reduced Rho activity substantially, i.e., to 49% of the activity measured in control cells (Fig. 2C). Together with the data shown in Fig. 1, these results demonstrated the previously unknown role of Cdh1 as a regulator of Rho GTPase.

Cdh1 depletion led to p190 RhoGAP accumulation. p190 RhoGAP (p190) is ubiquitously expressed in various tissues and functions exclusively toward Rho *in vivo*. Furthermore, p190 activity accounts for ~60% of the total RhoGAP activity when activity is assessed in fibroblast cell extracts (52). We observed a significant reduction of actin stress fiber formation in $Cdh1^{GT/GT}$ MEFs, which is consistent with a phenotype of Rho inhibition (Fig. 1A). Hence, we assumed that APC/C^{Cdh1} may target p190 directly as a substrate for degradation. To test this possibility, we compared the expression levels of p190 in $Cdh1^{GT/GT}$ MEFs with those of wild-type cells using immunoblot analysis. Consistent with the results reported for the known APC/C^{Cdh1} substrate Skp2 (6, 56), p190 accumulated substantially in $Cdh1^{GT/GT}$ MEFs (1.94-fold compared with wild-type MEFs) (Fig. 3A). We used quantitative real-time PCR analysis to confirm that the observed difference in p190 abundance was not due to transcriptional upregulation (Fig. 3B). To further examine whether Cdh1 had a negative impact on the expression of the p190 protein, we interfered with Cdh1 function in HeLa cells via transfection of an siRNA oligonucleotide against Cdh1 or of a dominant negative mutant Cdh1 expression vector (54) and analyzed their effect on p190 abundance. Impairment of Cdh1 function led to the accumulation of the p190 protein (Fig. 3C and D). Simple overexpression of wild-type Cdh1 had no effect on the expression levels of p190 or on cellular morphology (Fig. 3D and data not shown), which implies that exogenously induced Cdh1 did not activate APC/C efficiently. To address this issue, we depleted early mitosis inhibitor 1 (Emi1), which is an inhibitor of APC/C^{Cdh1}, to catalytically activate endogenous APC/C^{Cdh1} in interphase HeLa cells (12, 27). We analyzed HeLa cells transfected with siRNA oligonucleotides against Emi1 and found that p190 expression levels were reduced significantly in these cells (Fig. 3E, first panel). Another known target of APC/C^{Cdh1}, cyclin B1, was also decreased after Emi1 depletion (Fig. 3E, arrow in the second panel). Furthermore, the decreased p190 levels in Emi1-depleted HeLa cells were restored by proteasome inhibitor treatment (Fig. 3E). These results support the notion that APC/C^{Cdh1} regulated p190 abundance via the ubiquitin-proteasome system.

A previous study indicated that the levels of p190 oscillate in a cell cycle-dependent manner; they are elevated from interphase to mid-mitosis and decline after entry into late mitosis (45). Therefore, loss of Cdh1 function during the cell cycle, especially on mitotic exit, may affect the abundance of p190. To rule out this possibility, we analyzed the cell cycle profiles of $Cdh1^{GT/GT}$ MEFs and Cdh1-depleted HeLa cells using flow cytometry. Consistent with a previous report (15), the Cdh1-depleted cell population contained a slightly elevated number of cells that were in the G_2/M phase of the cell cycle (Fig. 3F), which suggests slower mitotic progression. As a shortened mitosis can cause secondary p190 accumulation, these results indicate that cell cycle alteration in Cdh1-depleted cells may be unfavorable to p190 protein accumulation. Therefore, the role of Cdh1 during the cell cycle seems to be independent from the regulation of p190 abundance.

APC/C^{Cdh1}-mediated ubiquitination of p190. Cdh1 recognizes and binds target motifs on its substrate (35). The destruction (D) and KEN boxes are most prominent among the targeting motifs of APC/C substrates for degradation. p190 has five D boxes and two KEN boxes in its full sequence (Fig. 4A). To determine whether p190 was a direct target of APC/C^{Cdh1}, we performed an *in vitro* binding assay using several p190 mutants. As shown in Fig. 4B, both full-length p190 and the middle domain (MD) of p190 were coprecipitated with *in vitro* translated Cdh1 (Fig. 4B). Furthermore, deletion mutants containing only KEN-box (MD-N) and D-boxes (MD-C) were also

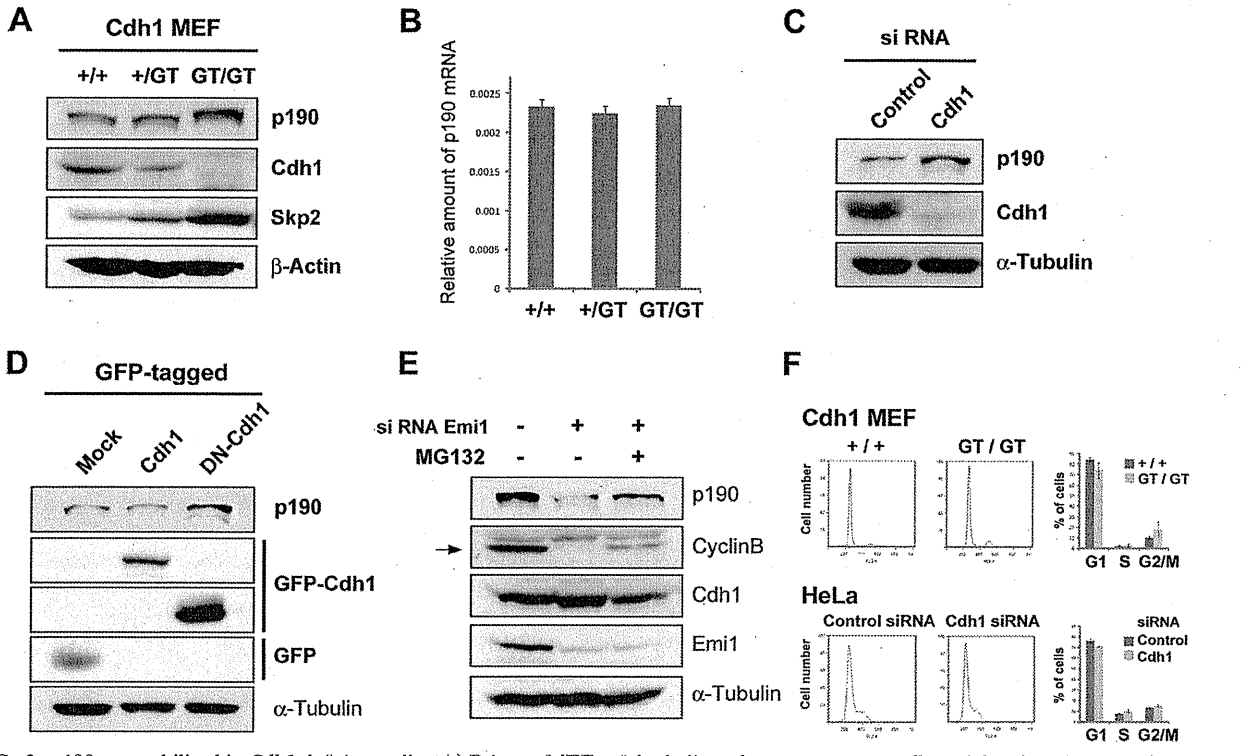

FIG. 3. p190 was stabilized in *Cdh1*-deficient cells. (A) Primary MEFs of the indicated genotypes were collected, lysed, and immunoblotted for endogenous p190, Cdh1, and Skp2. β-Actin levels are shown as a loading control. Each experiment was conducted in triplicate, and the immunoblots presented here are representative runs. (B) An abundance of p190 proteins was regulated posttranslationally. Total RNA was isolated from MEFs of the indicated genotypes and subjected to quantitative RT-PCR analysis of the p190 mRNA. Data were normalized to the levels of GAPDH mRNA and represent means ± standard deviations from three independent experiments. (C) Accumulation of p190 in *Cdh1*-depleted HeLa cells. HeLa cells were transfected with either control or Cdh1 siRNA oligonucleotides. After 48 h of culture, cells were harvested and examined for the expression levels of p190, Cdh1, and α-tubulin using immunoblotting analysis. (D) HeLa cells were transfected with GFP-tagged full-length Cdh1 or DN-Cdh1 expression vectors. Cells were lysed and processed through immunoblotting using antibodies against p190, GFP, and α-tubulin. (E) Cdh1 activation caused a reduction in the levels of p190. HeLa cells transfected with control or Emi1 siRNA oligonucleotides were cultured for 48 h in the absence (−) or presence (+) of MG132. Cell lysates were subjected to SDS-PAGE and immunoblot analysis using the indicated antibodies. Emi1 depletion led to Cdh1 activation, as evidenced by the degradation of its target, cyclin B (arrow, middle lane). (F) Flow cytometric analysis of the cell cycle. Asynchronous MEFs with the indicated genotypes and HeLa cells that were transfected with either control or Cdh1 siRNA oligonucleotides for 24 h were stained with propidium iodide and were then subjected to flow cytometry. The percentage of cells in each phase of the cell cycle is shown.

bound to Cdh1 (Fig. 4B), which indicates the relevance of each box for the interaction with Cdh1. We next examined the *in vivo* interaction between Cdh1 and p190. Immunoprecipitation of the lysate that expressed GFP-fused full-length Cdh1 using the p190 antibody led to the identification of exogenous Cdh1 in the complex (Fig. 4C). To confirm the physiological interaction between these proteins, we prepared a Cdh1-specific antibody by immunizing rabbits with mouse Cdh1 N-terminal peptides. Using this polyclonal antibody, we found that endogenous p190 coprecipitated with endogenous Cdh1 (Fig. 4D).

We next examined whether the abundance of p190 was regulated via the ubiquitin–proteasome system. Coexpression of GFP-p190 with HA-tagged ubiquitin in 293T cells revealed that p190 was ubiquitinated predominantly in the presence of the proteasome inhibitor (Fig. 5A), which supports the notion that p190 is ubiquitinated *in vivo* (45). However, 293T cells transfected with an siRNA oligonucleotide against Cdh1 exhibited a substantial reduction in the ubiquitination of endogenous p190 (Fig. 5B) to ~60% of that observed in control cells (Fig. 5C). Furthermore, the decrease in the ubiquitination of p190 in immortalized $Cdh1^{GT/GT}$ MEFs was restored by the addition of wild-type Cdh1 in a dose-dependent manner (Fig. 5D). We next examined whether the APC/C^{Cdh1} complex ubiquitinated p190 directly using an *in vitro* ubiquitination assay. We incubated immunopurified HeLa APC/C with or without recombinant His-tagged full-length Cdh1 protein purified from Sf9 cells. The resultant APC/C^{Cdh1} complex was analyzed for its ability to support the ubiquitination of *in vitro* translated p190 in a reconstituted reaction mixture containing purified E1 and E2 enzymes (22). As shown in Fig. 5E, APC/C ubiquitinated p190 effectively *in vitro* when Cdh1 was present in the reaction mixture.

Cdh1 regulated cellular motility via control of p190 abundance. As the coordinated regulation of Rho activity is important for cell migration (13), we investigated whether Cdh1 deficiency affected cellular movement. The migration ability of Cdh1 knockdown HeLa cells was examined using a Boyden chamber migration assay. Serum-deprived siRNA-transfected HeLa cells were plated onto the membrane of a Boyden chamber in the absence of any stimuli and were allowed to migrate

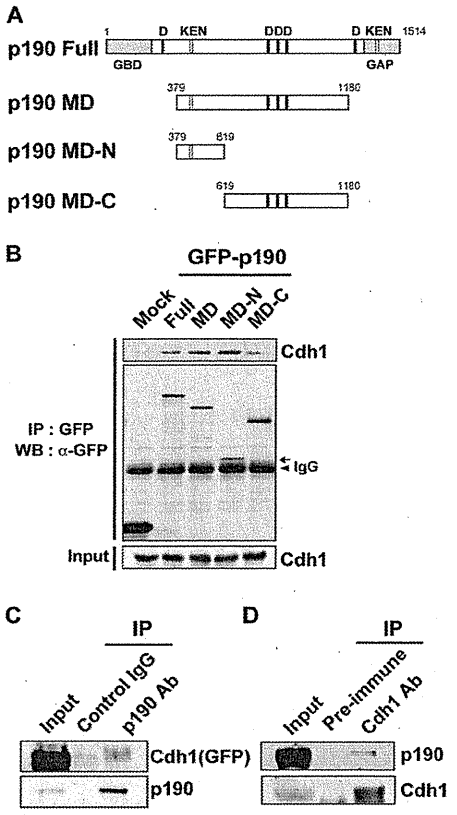

FIG. 4. The middle domain of p190 interacted with Cdh1. (A) Schematic representations of the structure of p190 and its derived mutants. MD, middle domain; GBD, GTP-binding domain; GAP, GTPase-activating domain. (B) *In vitro* binding assay. The indicated GFP-p190 proteins expressed in 293T cells were immunopurified, immobilized on protein A beads (Dynal), and incubated with *in vitro* translated Cdh1. The resulting immunocomplex was analyzed using avidin-HRP to detect the bound biotin-Cdh1. The arrow indicates the MD-N mutant for p190. The arrowhead indicates IgG. (C) Lysates from 293T cells transfected with GFP-tagged full-length Cdh1 were immunoprecipitated using control rabbit IgG or an antibody (Ab) against p190. These immunoprecipitates were then fractionated by SDS-PAGE and immunoblotted using an anti-GFP antibody (top) or an anti-p190 antibody (bottom). (D) *In vivo* coimmunoprecipitation of p190 with Cdh1. Lysates from 293T cells were immunoprecipitated with rabbit preimmune serum or serum against Cdh1. These immunoprecipitates were then fractionated by SDS-PAGE and immunoblotted using anti-p190 (top) or anti-Cdh1 (bottom) antibodies. IP: immunoprecipitation; WB, Western blotting.

for 24 h. Unstimulated HeLa cells exhibited virtually no motility (Fig. 6C, first bar). Stimulation of HeLa cells with FBS led to an increase in their migratory activity compared with unstimulated HeLa cells (Fig. 6A, left panel, and C, second bar). Importantly, Cdh1 knockdown cells exhibited very low motility, even when stimulated by FBS (Fig. 6A, middle panel, and C, third bar). To determine if Cdh1 and its substrate p190 acted in a linear pathway to regulate cellular motility, we performed an epistatic analysis of the effects of Cdh1 and p190 knockdown on a cell migration assay. We optimized co-knockdown conditions to deplete p190 in *Cdh1*-knockdown cells to levels comparable to those of control cells (Fig. 6B). The combination of both Cdh1 and p190 RNAi rescued the motility defect of Cdh1 knockdown HeLa cells significantly to ~110% of the level observed in control cells (Fig. 6A, right panel, and C, fourth bar).

Given that p190-mediated regulation of Rho is important for cell migration, how does Cdh1 affect p190 activity? It is known that the activity of p190 is regulated by phosphorylation (5, 30). We speculated that the level of expression of p190 may also be a key factor to control its RhoGAP activity. To examine this hypothesis, we analyzed the distribution of F-actin in p190 knockdown cells at different time points. As shown in Fig. 6D and E, the extent of stress fiber formation of p190 knockdown HeLa cells was inversely correlated with the abundance of p190. Furthermore, when p190 was exogenously overexpressed in MEFs or NIH 3T3 cells, these cells had reduced stress fibers and exhibited reorganized cortical actin compared with surrounding nontransfected cells (Fig. 6F, upper row, and G) as in dominant negative Cdh1-expressing cells (Fig. 1D and F). These results suggest that p190 abundance plays a key role in its RhoGAP activity. We also confirmed that the actin phenotype of $Cdh1^{GT/GT}$ MEFs was rescued by introducing wild-type Cdh1 (Fig. 6F, lower row). These findings are consistent with the notion that APC/C^{Cdh1} and p190 operate in a linear pathway, where p190 acts downstream of APC/C^{Cdh1} in the control of Rho GTPase.

Physiological role of Cdh1 during murine development. To analyze the relevance of Cdh1-mediated regulation of Rho *in vivo*, we analyzed $Cdh1^{GT/GT}$ mice. Among the 152 mice that were the progeny of the intercross of $Cdh1^{+/GT}$ mice, no $Cdh1^{GT/GT}$ animals were detected at weaning (see Table S1 in the supplemental material), which confirmed that homozygous loss of *Cdh1* resulted in embryonic death (15, 24). To determine the timing and nature of this mortality, we examined the morphology and viability of embryos from timed $Cdh1^{+/GT}$ intercrosses. Viable embryos were defined by the detection of a heartbeat at 11.5 to 13.5 dpc. The number of viable $Cdh1^{GT/GT}$ embryos decreased with developmental progression, with none remaining alive at 13.5 dpc (see Table S1). These results thus suggest that embryonic death was initiated at around 10.5 to 12.5 dpc. We also confirmed that the death of $Cdh1^{GT/GT}$ embryos was attributable to the *Cdh1* GT using a KI rescue experiment (see Fig. S2 in the supplemental material).

The mouse placenta consists of three layers, which, starting from the embryonic side, are known as the labyrinth, the spongiotrophoblast, and the trophoblast giant cell (TGC) layers (Fig. 7A, top panel) (34). In contrast with the thin layer of TGCs present beneath the maternal decidua in wild-type placentas, cells with giant nuclei were not detected in $Cdh1^{GT/GT}$ placentas, as assessed by either hematoxylin-eosin or Feulgen staining (see Fig. S3 in the supplemental material). This implies that the endoreplication of TGC was compromised in $Cdh1^{GT/GT}$ placentas (15, 24). Cdh1 was expressed in the labyrinth layer of $Cdh1^{+/GT}$ placentas, as revealed by whole-mount X-Gal staining (see Fig. S3). Hematoxylin-eosin staining of $Cdh1^{GT/GT}$ placentas at 12.5 or 13.5 dpc revealed the presence of frequent abnormal thrombi in the labyrinth layers (Fig. 7A, middle panel, and B). Furthermore, the labyrinth layer of $Cdh1^{GT/GT}$ placentas exhibited an abnormal vasculature compared with that of their wild-type counterparts (Fig.

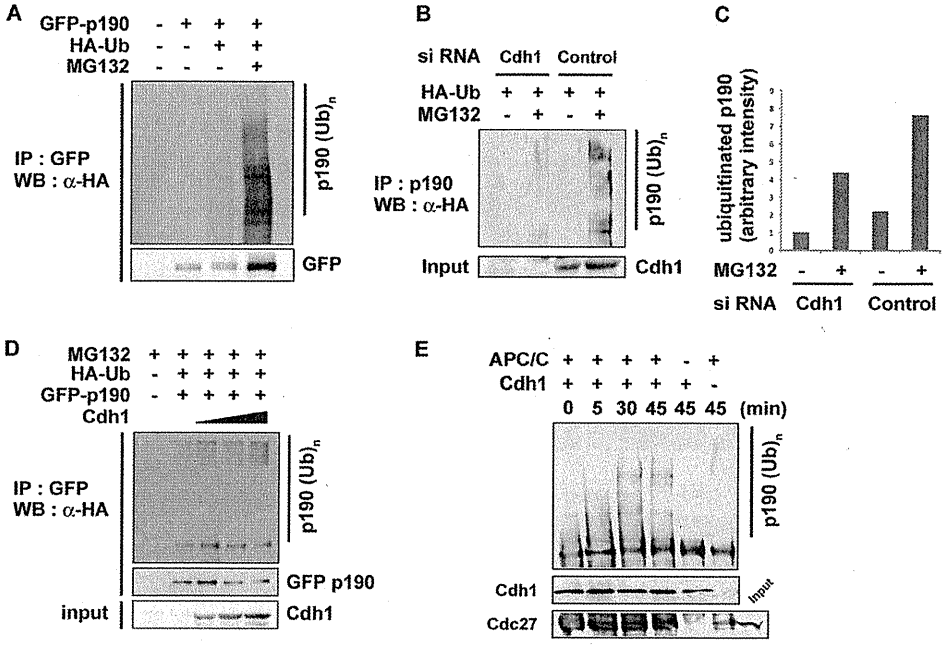

FIG. 5. APC/C^{Cdh1}-mediated ubiquitination of p190. (A) *In vivo* ubiquitination of p190. 293T cells were transfected with the GFP–full-length p190 expression plasmid or control vector, together with an HA-ubiquitin expression plasmid in the presence or absence of MG132. Lysates were immunoprecipitated (IP) with an anti-GFP antibody and were immunoblotted (Western blotting [WB]) using anti-HA (α-HA) and anti-GFP antibodies. (B) 293T cells transfected with either control or Cdh1 siRNA oligonucleotides for 48 h were subjected to an *in vivo* ubiquitination assay, as described for panel A. (C) Quantification of the ubiquitinated p190 protein in panel B was performed using densitometry. The value obtained for Cdh1 siRNA-transfected cells without MG132 treatment was set as 1. (D) Immortalized $Cdh1^{GT/GT}$ MEFs were transfected with GFP-full-length p190, HA-ubiquitin (Ub), and full-length Cdh1 expression vectors. *In vivo* ubiquitination of p190 was evaluated as described for panels A and B. (E) *In vitro* ubiquitination assay. APC/C immunoprecipitated from HeLa cell lysates was conjugated with recombinant Cdh1 protein and was then subjected to an *in vitro* ubiquitination assay, as described in Materials and Methods. *In vitro* translated full-length p190 was used as a substrate. The reaction was terminated at the indicated time points. Ubiquitinated p190 was detected by immunoblotting with anti-p190 antibody (top panel). Recombinant His-Cdh1 protein used for APC/C binding was immunoblotted using anti-His antibody (middle). The presence of APC/C complex in each reaction product was confirmed by Western blotting against cdc27 (bottom). The input lane represents 0.5% of HeLa cell lysate used for immunoprecipitation.

7A). These phenotypes were similar to *ROCK II* (also known as Rho-kinase or ROK α) knockout (KO) mice (49).

To examine whether placental insufficiency was a central cause of embryonic lethality, we performed tetraploid complementation rescue experiments (Fig. 7A, bottom panel; see also Fig. S4 in the supplemental material). We found that $Cdh1^{GT/GT}$ embryos survived beyond the organogenesis stage to 18.5 dpc in this system. The placental deficiencies of $Cdh1^{GT/GT}$ mice somewhat resembled those of *ROCK II* KO mice; however, in contrast to what was observed in *ROCK II* KO mice, blood clots in peripheral limbs were not observed in $Cdh1^{GT/GT}$ animals. Eyes open at birth and omphalocele are significant phenotypes of *ROCK I* (also known as ROK β) KO mice (44). During normal mouse development, eyelid closure occurs between 15.5 and 16.5 dpc via extension of the ridges of the epithelium at its periphery (14). To explore whether Cdh1 deficiency caused a defect in this developmental process, we analyzed $Cdh1^{GT/GT}$ embryos rescued using tetraploid complementation experiments. We used wild-type ES cell lines that were established concomitantly with $Cdh1^{GT/GT}$ ES cell lines (see Materials and Methods) as a control for tetraploid aggregation. Tetraploid complementation itself affects the timing of eyelid closure, as all wild-type embryos examined ($n = 4$) had open eyelids at 15.5 dpc; however, this was reduced to 22.2% of embryos ($n = 9$) at 18.5 dpc (Fig. 7C to F). In contrast, 83.3% of $Cdh1^{GT/GT}$ embryos exhibited an open-eye phenotype ($n = 10$) at 18.5 dpc, which suggests a significant role for Cdh1 in eyelid closure (Fig. 7C to F). Conversely, we did not observe increased omphalocele in $Cdh1^{GT/GT}$ embryos (data not shown). Eyelid closure is regulated by complicated mechanisms, as other signaling pathways, such as the mitogen-activated protein (MAP) kinase cascade, are also involved in this process (44). To explore whether Cdh1 regulated eyelid closure via the Rho/ROCK pathway, we analyzed the abundance of p190 in the eyelid epithelial sheet. Immunohistochemical analysis of p190 showed that staining for p190 was more pronounced in the eyelid epithelial sheet of $Cdh1^{GT/GT}$ embryos than in wild-type embryos (Fig. 7G). Furthermore, p190 accumulated in the brain and spinal cord of $Cdh1^{GT/GT}$ embryos, where p190 mRNA is expressed specifically at high levels (10) (Fig. 7H). These results strongly suggest that Cdh1 is an important regulator of the *in vivo* Rho/ROCK signaling via p190.

DISCUSSION

In the present study, we identified a novel function for the APC/C activator Cdh1 on the regulation of Rho subfamily GTPases. Rho promotes the formation of actin stress fibers

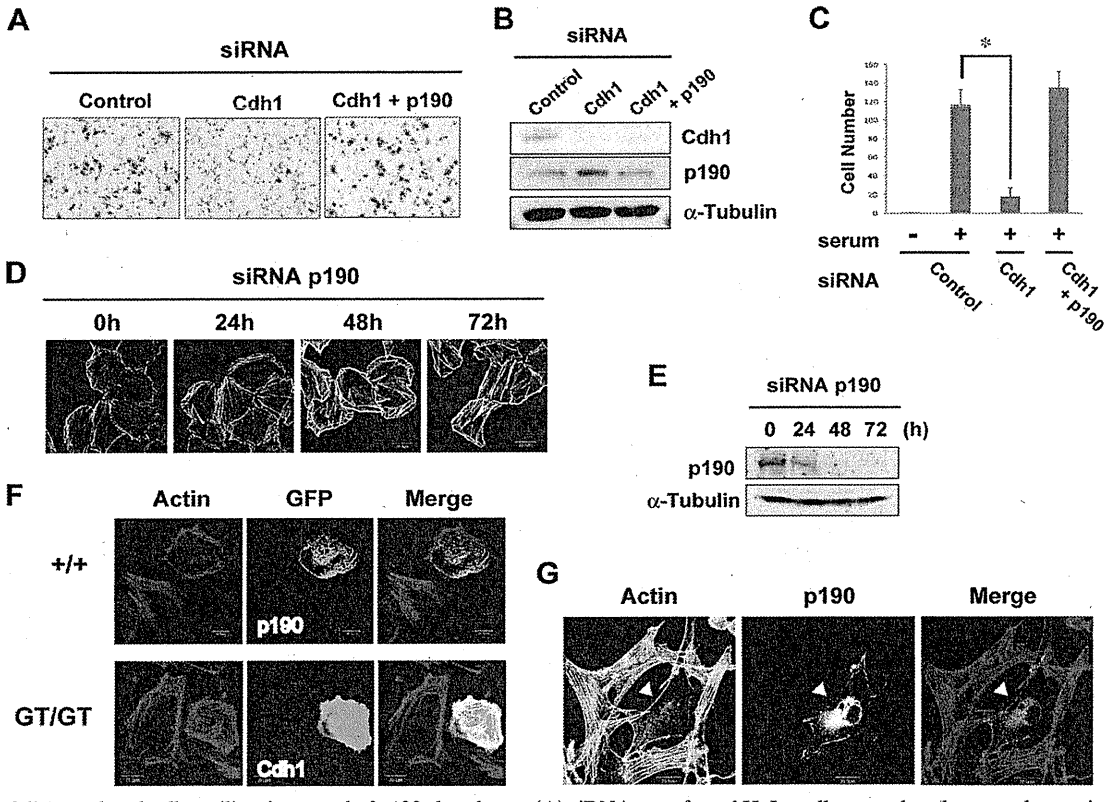

FIG. 6. Cdh1 regulated cell motility via control of p190 abundance. (A) siRNA-transfected HeLa cells were placed on membranes in serum-free medium after 48 h of culture and were allowed to migrate in a Boyden chamber for 24 h, either in the absence of any stimuli or in the presence of 10% FBS. Membranes were then fixed and stained with 50% Giemsa solution in PBS. Data shown were representative of migrating cells transfected with the indicated siRNA oligonucleotides. (B) The levels of Cdh1 and p190 in cells subjected to a Boyden chamber assay were assessed by immunoblot analysis using anti-Cdh1 and anti-p190 antibodies. The corresponding α-tubulin levels are shown as a loading control. (C) Migration was assessed as the number of cells that invaded the membrane after 24 h of incubation. Data represented mean values ± standard errors of the means from measurements performed in triplicate from three independent experiments using HeLa cells (*, $P < 0.05$, Student's two-tailed t test). (D) HeLa cells were transfected with siRNA oligonucleotides against p190 and cultured for 0 to 48 h in the medium containing 10% FBS. After 48 h, the cell medium was replaced with serum-free DMEM-F12. Cells were fixed and stained with Alexa Fluor 488-phalloidin at the indicated times. (E) HeLa cells were transfected and cultured as described for panel D. Cells were harvested and examined for the expression levels of p190 and α-tubulin using immunoblot analysis. (F) Primary wild-type (upper row) and *Cdh1*$^{GT/GT}$ (lower row) MEFs were transfected for 24 h with GFP-p190 and GFP–wild-type Cdh1, respectively. Cells were fixed and stained with rhodamine-phalloidin. (G) NIH 3T3 cells were transfected for 24 h with GFP-p190. Cells were fixed and stained with Alexa Fluor 488-phalloidin. The arrowhead indicates p190 transfected cells. Bars, 100 μm (A) and 20 μm (D, F, and G).

and FAs by activating its downstream effectors, i.e., ROCK and mDia (mammalian homolog of the *Drosophila* gene *Diaphanous*) (32). ROCK induces stress fiber formation via the phosphorylation of myosin phosphatase and LIM kinase in nonmuscle cells (2). It has been reported that ROCK inhibition blocks myosin light chain phosphorylation and the subsequent formation of stress fibers in the center, but not at the periphery, of cells (50). Cdh1-depleted cells significantly reduced the formation of actin filament bundles at the cell body; however, it was retained at cell periphery (Fig. 1B and E), which implies the presence of ROCK suppression in these cells. mDia also regulates actin filament formation and adhesion turnover via the mobilization of adenomatous polyposis coli and c-Src (58). FAs are specialized adhesive structures in which integrin, a receptor of the extracellular matrix, and numerous signaling components are concentrated (11). The importance of the actin cytoskeleton in FA assembly has been demonstrated in experiments where inhibition of the actin-myosin interaction promotes disassembly of FAs (42). Consistently, we found that the Cdh1 deficiency caused a reduction of both stress fiber and FA assembly, with a decreased level of active Rho (Fig. 1 and 2). This Rho-mediated response acts downstream of the signaling activated by growth factors (38, 42). Serum starvation of cells transfected with Cdh1 siRNA resulted in further attenuation of the assembly of stress fibers and FAs compared with cells with Cdh1 knockdown only (Fig. 1C), which indicates that multiple signals, including the Cdh1/p190 axis, seem to converge during Rho regulation. Rho-mediated actin cytoskeleton formation is controlled at multiple levels. Elevation of cyclic AMP (cAMP) levels and the consequent activation of protein kinase A (PKA) lead to loss of stress fibers and FAs via the phosphorylation of the myosin light chain kinase and Rho (42). It was reported that PKA also phosphorylates APC/C and inhibits its ubiquitination activity, even in the presence of Cdh1 (21). Therefore, we could speculate that cAMP/PKA regulates the actin cytoskeleton also via an APC/C^{Cdh1}/p190/Rho pathway.

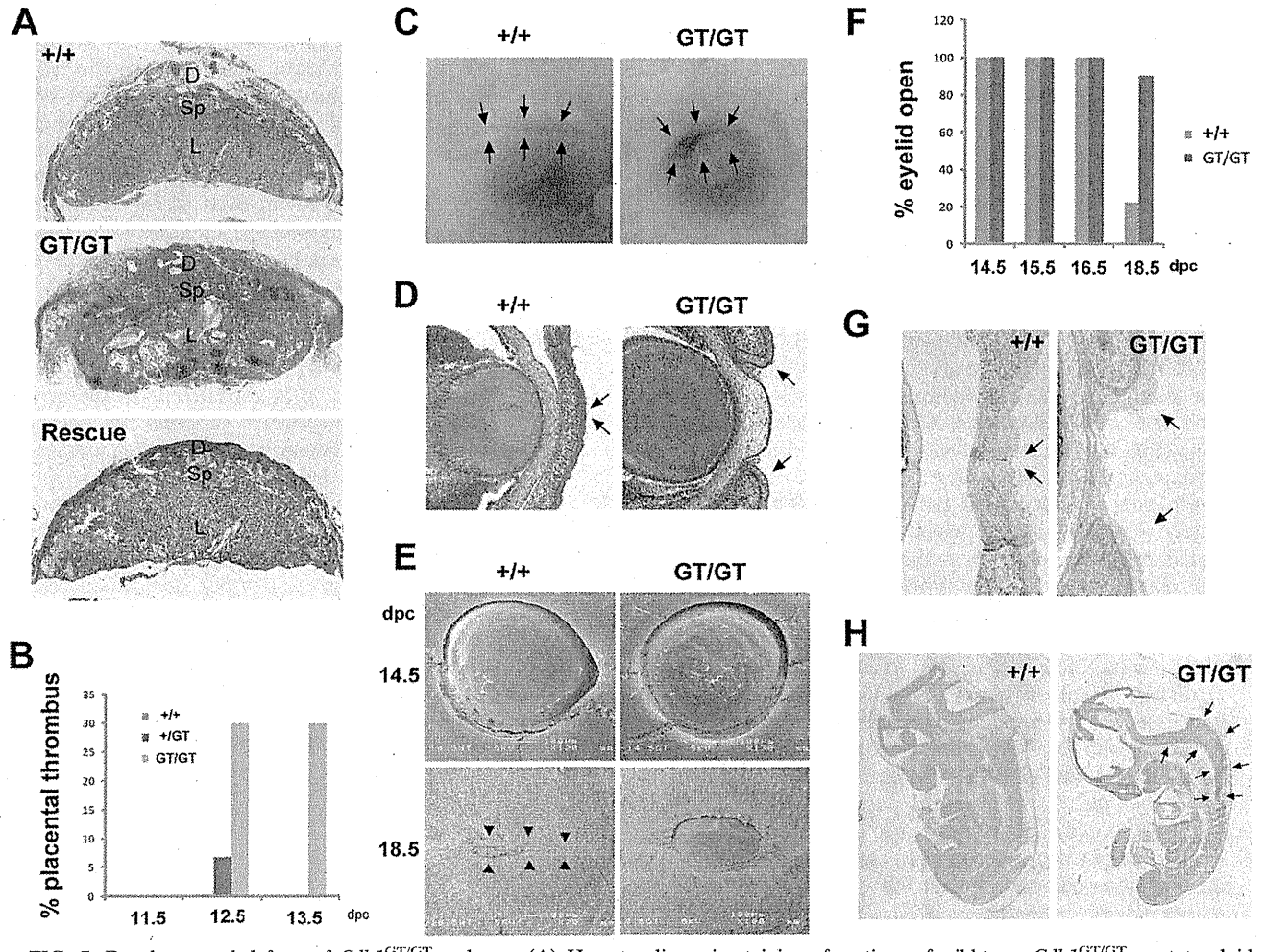

FIG. 7. Developmental defects of *Cdh1*$^{GT/GT}$ embryos. (A) Hematoxylin-eosin staining of sections of wild-type, *Cdh1*$^{GT/GT}$, or tetraploid complementation-rescued placentas at 12.5 dpc. The asterisk indicates thrombus in the labyrinth layer. D, decidua; Sp, spongiotrophoblast layer; L, labyrinth layer. (B) Percentage of placentas with thrombus formation at the indicated dpc. Placentas with thrombus that had a diameter larger than 500 μm (longest diameter) were judged as positive. The number of placentas analyzed was as follows: at 11.5 dpc, *Cdh1*$^{+/+}$, 5; *Cdh1*$^{GT/+}$, 8; and *Cdh1*$^{GT/GT}$, 7; at 12.5 dpc, *Cdh1*$^{+/+}$, 6; *Cdh1*$^{GT/+}$, 15; and *Cdh1*$^{GT/GT}$, 10; at 13.5 dpc, *Cdh1*$^{+/+}$, 8; Cdh1$^{GT/+}$, 8; and *Cdh1*$^{GT/GT}$, 10. (C) The eyes of wild-type and *Cdh1*$^{GT/GT}$ mice at 18.5 dpc were obtained from tetraploid complementation. The arrows indicate the margin of the eyelid. (D) Hematoxylin-eosin staining of transverse eye sections from 18.5-dpc embryos, as in panel C. The arrows indicate the margin of the eyelid. (E) Scanning electron micrographs of the eyes of wild-type or *Cdh1*$^{GT/GT}$ rescue embryos at the indicated dpc. The arrowheads indicate eyelid fusion in wild-type embryos. (F) Percentage of embryos with eyelids open at the indicated dpc. The number of embryos analyzed was as follows: at 14.5 dpc, *Cdh1*$^{+/+}$, 2; and *Cdh1*$^{GT/GT}$, 2; at 15.5 dpc, *Cdh1*$^{+/+}$, 8; *Cdh1*$^{GT/GT}$, 5; at 16.5 dpc, *Cdh1*$^{+/+}$, 8; and *Cdh1*$^{GT/GT}$, 3; at 18.5 dpc, *Cdh1*$^{+/+}$, 9; and *Cdh1*$^{GT/GT}$, 10. (G) Immunohistochemical staining of p190 in transverse sections of the eyelid of wild-type and *Cdh1*$^{GT/GT}$ rescue embryos at 18.5 dpc. The arrows indicate the margin of the eyelid. (H) Sagittal sections of rescue embryos at 18.5 dpc were stained with an anti-p190 antibody. The arrows indicate p190 staining in the central nervous system of *Cdh1*$^{GT/GT}$ embryos. Bars, 50 μm (D) and 100 μm (E).

p190, which is a Rho family GTPase-activating protein, has been reported to account for a substantial fraction of the total inhibitory activity of Rho in cultured cells (52). RhoGAPs are regulated by various mechanisms, including protein-protein interactions, phospholipid modification, phosphorylation, subcellular translocation, and proteolytic degradation (7, 30). The Src-mediated phosphorylation of p190 promotes its RhoGAP activity, whereas ROCK-mediated phosphorylation of p190 leads to its inactivation via the inhibition of its binding to Rnd (5, 30). In addition to phosphorylation, our results suggested that control of the abundance of p190 was another regulatory mechanism of its activity (Fig. 6D to G).

p190 expression is not constant throughout the cell cycle (45). p190 expression decreases during late mitosis, and this reduction is dependent on ubiquitin-mediated protein degradation (45). APC/C^{Cdh1} is a strong E3 ubiquitin ligase candidate for p190 as the timing of APC/C^{Cdh1} activation fits well with the timing of p190 degradation. However, this has not been proven previously. In this study, we presented data that support our hypothesis as Cdh1 formed a physical complex with p190. We also found that Cdh1 stimulated the efficient

ubiquitination and degradation of p190, both *in vitro* and *in vivo* (Fig. 5). Su et al. proposed that the reduction of endogenous p190 levels during late mitosis is linked to completion of cytokinesis. Cytokinesis is driven by an actin and myosin contractile ring. Constitutive inhibition and activation of Rho block cytokinesis, which suggests that a complex regulation of Rho activity is required for the process (13). Constitutive overexpression of p190 in breast cancer cells leads to multinucleation, which is often caused by cytokinesis failure and is reminiscent of the phenotype of *Cdh1*-null fibroblasts (15, 45). Therefore, Cdh1 may regulate not only cell motility but also cytokinesis via p190.

p190 has five D boxes and two KEN boxes (Fig. 4A), which are degradation motifs that are recognized by APC/C^{Cdh1} (35). Our mutational analysis indicated that KEN and D boxes within the MD region were relevant for the interaction with Cdh1 (Fig. 4B). Cdh1 effectively stimulated ubiquitination and subsequent degradation of p190 (Fig. 5). However, Cdh1 knockdown did not inhibit the ubiquitination of p190 completely (Fig. 5B and C), which suggests that several other candidate E3 ligases, such as the Skp1-cullin-F-box complex, may also be involved in the process. Thus, our results suggest that APC/C^{Cdh1} is a major, but not exclusive, E3 ligase for p190. Further analysis will be required to explore the exact molecular mechanism of control of p190 abundance.

All Rho isoforms (RhoA, -B, and -C) induce stress fiber formation when overexpressed in fibroblasts (18). *RhoB*-null and *RhoC*-null mice are viable and have no major developmental defects (17, 26). The significance of RhoA in mammalian development is unknown because of a lack of *RhoA* KO mice (18). It is difficult at present to understand the developmental role of Cdh1 in terms of its correlation with Rho as we are unable to compare it with *RhoA* KO mice. Among the various downstream effectors of Rho, ROCKs were the first to be identified and appeared to mediate a significant proportion of the Rho signals (2, 39). Therefore, comparison of $Cdh1^{GT/GT}$ mice with *ROCK*-deficient mice may be useful for the elucidation of the physiological roles of Cdh1. *ROCK* KO mice have been generated, and the involvement of ROCK in the developmental process has been analyzed (44, 49). Most *ROCK* $I^{-/-}$ mice die soon after birth, and homozygous embryos exhibit failed eyelid and ventral wall closure (44). Most *ROCK* $II^{-/-}$ mice also exhibit embryonic lethality after 13.5 dpc and show defects in the placental labyrinth layer, with disruptive architecture and extensive thrombus formation (49). In the present study, the developmental failures observed in $Cdh1^{GT/GT}$ embryos have many similarities with those of both *ROCK* $I^{-/-}$ and *ROCK* $II^{-/-}$ mice. Cdh1 was highly expressed in the labyrinth layer of the placenta, similarly to ROCK II (see Fig. S3 in the supplemental material). A disorganized structure and an increased frequency of thrombus formation were found in the labyrinth layer of $Cdh1^{GT/GT}$ placenta (Fig. 7A and B). Loss of Cdh1 leads to embryonic lethality because of placental insufficiency at midgestation, which happens earlier than in *ROCK*-null embryos (15, 24). One possible reason for these differences in lethal timing is that *ROCK* KO mice have no TGC abnormalities (44, 49). Both the labyrinth and the TGC layer were compromised in *Cdh1*-deficient placentas, which may cause a more severe phenotype than that of *ROCK*-null embryos. We also confirmed the significance of the placenta in $Cdh1^{GT/GT}$ embryonic lethality using tetraploid complementation rescue. This technique allowed $Cdh1^{GT/GT}$ embryos to survive until birth; nevertheless, these embryos showed a delayed timing of eyelid closure compared with that of their normal counterparts. Embryos derived from wild-type ES cell aggregation resulted in delayed eyelid closure compared with those derived from normal pregnancy (44); however, $Cdh1^{GT/GT}$ embryos showed an even slower timing, which seems to rule out the possibility of an effect of the artificial defects of the delay associated with embryonic manipulation (Fig. 7C to F). The p190 mRNA is expressed abundantly in the central nervous system during mouse development (10). We found that the p190 protein was highly expressed in the spinal cord of $Cdh1^{GT/GT}$ embryos (Fig. 7H). Furthermore, the p190 protein also accumulated in epithelial cells of the eyelid of $Cdh1^{GT/GT}$ mice (Fig. 7G), which supports our notion that Cdh1 may modulate the RhoA/ROCK signaling axis via p190 regulation during mouse development.

In summary, our findings provided new insights into the physiological roles of Cdh1. Cdh1 regulated Rho via a major RhoGAP, p190. Therefore, Cdh1 participated not only in cell cycle regulation but also in cell motility. Its functional interaction with Rho provides a broader functional perspective of Cdh1 under physiological and pathological conditions.

ACKNOWLEDGMENTS

We thank H. Sabe for the pEGFP full-length p190 expression vector, P. P. Pandolfi and T. Maeda for the pWZL-hyg-SV40 large T retrovirus vector, T. Shinoda for help in the quantitative analysis of fluorescent intensity, I. Ishimatsu and M. Nakata for technical assistance in the histological analyses, Y. Ito and N. Suzuki for animal maintenance, K. Arai for secretarial assistance, and M. Amano, S. Nakada, and all members of the Saya lab for helpful comments and discussions. We also thank the members of the Gene Technology Center and CARD at Kumamoto University for technical assistance and animal maintenance.

This study was supported by grants from the Ministry of Education, Culture, Sports, Science, and Technology (MEXT) of Japan (to S.K. [20590315 and 20058033] and H.S. [17013070]).

REFERENCES

1. **Almeida, A., J. P. Bolanos, and S. Moreno.** 2005. Cdh1/Hct1-APC is essential for the survival of postmitotic neurons. J. Neurosci. **25:**8115–8121.
2. **Amano, M., Y. Fukata, and K. Kaibuchi.** 2000. Regulation and functions of Rho-associated kinase. Exp. Cell Res. **261:**44–51.
3. **Araki, K., T. Imaizumi, K. Okuyama, Y. Oike, and K. Yamamura.** 1997. Efficiency of recombination by Cre transient expression in embryonic stem cells: comparison of various promoters. J. Biochem. **122:**977–982.
4. **Araki, K., N. Takeda, A. Yoshiki, Y. Obata, N. Nakagata, T. Shiroishi, K. Moriwaki, and K. Yamamura.** 2009. Establishment of germline-competent embryonic stem cell lines from the MSM/Ms strain. Mamm. Genome **20:**14–20.
5. **Arthur, W. T., L. A. Petch, and K. Burridge.** 2000. Integrin engagement suppresses RhoA activity via a c-Src-dependent mechanism. Curr. Biol. **10:**719–722.
6. **Bashir, T., N. V. Dorrello, V. Amador, D. Guardavaccaro, and M. Pagano.** 2004. Control of the SCF(Skp2-Cks1) ubiquitin ligase by the APC/C^{Cdh1} ubiquitin ligase. Nature **428:**190–193.
7. **Bernards, A., and J. Settleman.** 2004. GAP control: regulating the regulators of small GTPases. Trends Cell Biol. **14:**377–385.
8. **Bernards, A., and J. Settleman.** 2005. GAPs in growth factor signalling. Growth Factors **23:**143–149.
9. **Brandeis, M., and T. Hunt.** 1996. The proteolysis of mitotic cyclins in mammalian cells persists from the end of mitosis until the onset of S phase. EMBO J. **15:**5280–5289.
10. **Brouns, M. R., S. F. Matheson, K. Q. Hu, I. Delalle, V. S. Caviness, J. Silver, R. T. Bronson, and J. Settleman.** 2000. The adhesion signaling molecule p190 RhoGAP is required for morphogenetic processes in neural development. Development **127:**4891–4903.
11. **Clark, E. A., and J. S. Brugge.** 1995. Integrins and signal transduction pathways: the road taken. Science **268:**233–239.

12. **Di Fiore, B., and J. Pines.** 2007. Emi1 is needed to couple DNA replication with mitosis but does not regulate activation of the mitotic APC/C. J. Cell Biol. **177:**425–437.
13. **Etienne-Manneville, S., and A. Hall.** 2002. Rho GTPases in cell biology. Nature **420:**629–635.
14. **Findlater, G. S., R. D. McDougall, and M. H. Kaufman.** 1993. Eyelid development, fusion and subsequent reopening in the mouse. J. Anat. **183:**121–129.
15. **Garcia-Higuera, I., E. Manchado, P. Dubus, M. Canamero, J. Mendez, S. Moreno, and M. Malumbres.** 2008. Genomic stability and tumour suppression by the APC/C cofactor Cdh1. Nat. Cell Biol. **10:**802–811.
16. **Gieffers, C., B. H. Peters, E. R. Kramer, C. G. Dotti, and J. M. Peters.** 1999. Expression of the CDH1-associated form of the anaphase-promoting complex in postmitotic neurons. Proc. Natl. Acad. Sci. U. S. A. **96:**11317–11322.
17. **Hakem, A., O. Sanchez-Sweatman, A. You-Ten, G. Duncan, A. Wakeham, R. Khokha, and T. W. Mak.** 2005. RhoC is dispensable for embryogenesis and tumor initiation but essential for metastasis. Genes Dev. **19:**1974–1979.
18. **Heasman, S. J., and A. J. Ridley.** 2008. Mammalian Rho GTPases: new insights into their functions from in vivo studies. Nat. Rev. Mol. Cell Biol. **9:**690–701.
19. **King, R. W., J. M. Peters, S. Tugendreich, M. Rolfe, P. Hieter, and M. W. Kirschner.** 1995. A 20S complex containing CDC27 and CDC16 catalyzes the mitosis-specific conjugation of ubiquitin to cyclin B. Cell **81:**279–288.
20. **Konishi, Y., J. Stegmuller, T. Matsuda, S. Bonni, and A. Bonni.** 2004. Cdh1-APC controls axonal growth and patterning in the mammalian brain. Science **303:**1026–1030.
21. **Kotani, S., S. Tugendreich, M. Fujii, P. M. Jorgensen, N. Watanabe, C. Hoog, P. Hieter, and K. Todokoro.** 1998. PKA and MPF-activated Polo-like kinase regulate anaphase-promoting complex activity and mitosis progression. Mol. Cell **1:**371–380.
22. **Kraft, C., M. Gmachl, and J. M. Peters.** 2006. Methods to measure ubiquitin-dependent proteolysis mediated by the anaphase-promoting complex. Methods **38:**39–51.
23. **Kuninaka, S., M. Nomura, T. Hirota, S. Iida, T. Hara, S. Honda, N. Kunitoku, T. Sasayama, Y. Arima, T. Marumoto, K. Koja, S. Yonehara, and H. Saya.** 2005. The tumor suppressor WARTS activates the Omi/HtrA2-dependent pathway of cell death. Oncogene **24:**5287–5298.
24. **Li, M., Y.-H. Shin, L. Hou, X. Huang, Z. Wei, E. Klann, and P. Zhang.** 2008. The adaptor protein of the anaphase promoting complex Cdh1 is essential in maintaining replicative lifespan and in learning and memory. Nat. Cell Biol. **10:**1083–1089.
25. **Li, W., G. Wu, and Y. Wan.** 2007. The dual effects of Cdh1/APC in myogenesis. FASEB J. **21:**3606–3617.
26. **Liu, A. X., N. Rane, J. P. Liu, and G. C. Prendergast.** 2001. RhoB is dispensable for mouse development, but it modifies susceptibility to tumor formation as well as cell adhesion and growth factor signaling in transformed cells. Mol. Cell. Biol. **21:**6906–6912.
27. **Machida, Y. J., and A. Dutta.** 2007. The APC/C inhibitor, Emi1, is essential for prevention of rereplication. Genes Dev. **21:**184–194.
28. **Maeda, T., R. M. Hobbs, T. Merghoub, I. Guernah, A. Zelent, C. Cordon-Cardo, J. Teruya-Feldstein, and P. P. Pandolfi.** 2005. Role of the proto-oncogene Pokemon in cellular transformation and ARF repression. Nature **433:**278–285.
29. **Mitsunaga, K., K. Araki, H. Mizusaki, K.-i. Morohashi, K. Haruna, N. Nakagata, V. Giguère, K.-i. Yamamura, and K. Abe.** 2004. Loss of PGC-specific expression of the orphan nuclear receptor ERR-β results in reduction of germ cell number in mouse embryos. Mech. Dev. **121:**237–246.
30. **Mori, K., M. Amano, M. Takefuji, K. Kato, Y. Morita, T. Nishioka, Y. Matsuura, T. Murohara, and K. Kaibuchi.** 2009. Rho-kinase contributes to sustained RhoA activation through phosphorylation of p190A RhoGAP. J. Biol. Chem. **284:**5067–5076.
31. **Nagy, A.** 2003. Manipulating the mouse embryo: a laboratory manual, 3rd ed. Cold Spring Harbor Laboratory Press, Cold Spring Harbor, NY.
32. **Narumiya, S., M. Tanji, and T. Ishizaki.** 2009. Rho signaling, ROCK and mDia1, in transformation, metastasis and invasion. Cancer Metastasis Rev. **28:**65–76.
33. **Olofsson, B.** 1999. Rho guanine dissociation inhibitors: pivotal molecules in cellular signalling. Cell Signal **11:**545–554.
34. **Papaioannou, V. E., and R. Behringer.** 2005. Mouse phenotypes: a handbook of mutation analysis. Cold Spring Harbor Laboratory Press, Cold Spring Harbor, NY.
35. **Peters, J. M.** 2006. The anaphase promoting complex/cyclosome: a machine designed to destroy. Nat. Rev. Mol. Cell Biol. **7:**644–656.
36. **Reid, T., T. Furuyashiki, T. Ishizaki, G. Watanabe, N. Watanabe, K. Fujisawa, N. Morii, P. Madaule, and S. Narumiya.** 1996. Rhotekin, a new putative target for Rho bearing homology to a serine/threonine kinase, PKN, and rhophilin in the Rho-binding domain. J. Biol. Chem. **271:**13556–13560.
37. **Ren, X. D., W. B. Kiosses, and M. A. Schwartz.** 1999. Regulation of the small GTP-binding protein Rho by cell adhesion and the cytoskeleton. EMBO J. **18:**578–585.
38. **Ridley, A. J., and A. Hall.** 1992. The small GTP-binding protein rho regulates the assembly of focal adhesions and actin stress fibers in response to growth factors. Cell **70:**389–399.
39. **Riento, K., and A. J. Ridley.** 2003. Rocks: multifunctional kinases in cell behaviour. Nat. Rev. Mol. Cell Biol. **4:**446–456.
40. **Sahai, E., R. Garcia-Medina, J. Pouyssegur, and E. Vial.** 2007. Smurf1 regulates tumor cell plasticity and motility through degradation of RhoA leading to localized inhibition of contractility. J. Cell Biol. **176:**35–42.
41. **Schmidt, A., and A. Hall.** 2002. Guanine nucleotide exchange factors for Rho GTPases: turning on the switch. Genes Dev. **16:**1587–1609.
42. **Schoenwaelder, S. M., and K. Burridge.** 1999. Bidirectional signaling between the cytoskeleton and integrins. Curr. Opin. Cell Biol. **11:**274–286.
43. **Schwab, M., A. S. Lutum, and W. Seufert.** 1997. Yeast Hct1 is a regulator of Clb2 cyclin proteolysis. Cell **90:**683–693.
44. **Shimizu, Y., D. Thumkeo, J. Keel, T. Ishizaki, H. Oshima, M. Oshima, Y. Noda, F. Matsumura, M. M. Taketo, and S. Narumiya.** 2005. ROCK-I regulates closure of the eyelids and ventral body wall by inducing assembly of actomyosin bundles. J. Cell Biol. **168:**941–953.
45. **Su, L., J. M. Agati, and S. J. Parsons.** 2003. p190RhoGAP is cell cycle regulated and affects cytokinesis. J. Cell Biol. **163:**571–582.
46. **Sudakin, V., D. Ganoth, A. Dahan, H. Heller, J. Hershko, F. C. Luca, J. V. Ruderman, and A. Hershko.** 1995. The cyclosome, a large complex containing cyclin-selective ubiquitin ligase activity, targets cyclins for destruction at the end of mitosis. Mol. Biol. Cell **6:**185–197.
47. **Sudo, T., Y. Ota, S. Kotani, M. Nakao, Y. Takami, S. Takeda, and H. Saya.** 2001. Activation of Cdh1-dependent APC is required for G1 cell cycle arrest and DNA damage-induced G2 checkpoint in vertebrate cells. EMBO J. **20:**6499–6508.
48. **Taniwaki, T., K. Haruna, H. Nakamura, T. Sekimoto, Y. Oike, T. Imaizumi, F. Saito, M. Muta, Y. Soejima, A. Utoh, N. Nakagata, M. Araki, K. Yamamura, and K. Araki.** 2005. Characterization of an exchangeable gene trap using pU-17 carrying a stop codon-beta geo cassette. Dev. Growth Differ. **47:**163–172.
49. **Thumkeo, D., J. Keel, T. Ishizaki, M. Hirose, K. Nonomura, H. Oshima, M. Oshima, M. M. Taketo, and S. Narumiya.** 2003. Targeted disruption of the mouse Rho-associated kinase 2 gene results in intrauterine growth retardation and fetal death. Mol. Cell. Biol. **23:**5043–5055.
50. **Totsukawa, G., Y. Yamakita, S. Yamashiro, D. J. Hartshorne, Y. Sasaki, and F. Matsumura.** 2000. Distinct roles of Rock (Rho-Kinase) and Mlck in spatial regulation of Mlc phosphorylation for assembly of stress fibers and focal adhesions in 3t3 fibroblasts. J. Cell Biol. **150:**797–806.
51. **Tsubouchi, A., J. Sakakura, R. Yagi, Y. Mazaki, E. Schaefer, H. Yano, and H. Sabe.** 2002. Localized suppression of RhoA activity by Tyr31/118-phosphorylated paxillin in cell adhesion and migration. J. Cell Biol. **159:**673–683.
52. **Vincent, S., and J. Settleman.** 1999. Inhibition of RhoGAP activity is sufficient for the induction of Rho-mediated actin reorganization. Eur. J. Cell Biol. **78:**539–548.
53. **Visintin, R., S. Prinz, and A. Amon.** 1997. CDC20 and CDH1: A family of substrate-specific activators of APC-dependent proteolysis. Science **278:**460–463.
54. **Wan, Y., X. Liu, and M. W. Kirschner.** 2001. The anaphase-promoting complex mediates TGF-beta signaling by targeting SnoN for destruction. Mol. Cell **8:**1027–1039.
55. **Wang, H. R., Y. Zhang, B. Ozdamar, A. A. Ogunjimi, E. Alexandrova, G. H. Thomsen, and J. L. Wrana.** 2003. Regulation of cell polarity and protrusion formation by targeting RhoA for degradation. Science **302:**1775–1779.
56. **Wei, W., N. G. Ayad, Y. Wan, G. J. Zhang, M. W. Kirschner, and W. G. Kaelin, Jr.** 2004. Degradation of the SCF component Skp2 in cell-cycle phase G1 by the anaphase-promoting complex. Nature **428:**194–198.
57. **Yagi, T., T. Tokunaga, Y. Furuta, S. Nada, M. Yoshida, T. Tsukada, Y. Saga, N. Takeda, Y. Ikawa, and S. Aizawa.** 1993. A novel ES cell line, TT2, with high germline-differentiating potency. Anal. Biochem. **214:**70–76.
58. **Yamana, N., Y. Arakawa, T. Nishino, K. Kurokawa, M. Tanji, R. E. Itoh, J. Monypenny, T. Ishizaki, H. Bito, K. Nozaki, N. Hashimoto, M. Matsuda, and S. Narumiya.** 2006. The Rho-mDia1 pathway regulates cell polarity and focal adhesion turnover in migrating cells through mobilizing Apc and c-Src. Mol. Cell. Biol. **26:**6844–6858.

© Med Sci Monit, 2011; 17(2): PH7-11
PMID: 21278701

www.MEDSCIMONIT.COM
Public Health

Received: 2009.12.21
Accepted: 2010.07.07
Published: 2011.02.01

Authors' Contribution:
A Study Design
B Data Collection
C Statistical Analysis
D Data Interpretation
E Manuscript Preparation
F Literature Search
G Funds Collection

The incidence of hepatocellular carcinoma associated with hepatitis C infection decreased in Kyushu area

Naota Taura[1ABCDEFG], Nobuyoshi Fukushima[2ABCDEFG], Hiroshi Yatsuhashi[1ABCDEFG], Yuko Takami[3ABCDEFG], Masataka Seike[4ABCDEFG], Hiroshi Watanabe[5ABCDEFG], Toshihiko Mizuta[6ABCDEFG], Yutaka Sasaki[7ABCDEFG], Kenji Nagata[8ABCDEFG], Akinari Tabara[9ABCDEFG], Yasuji Komorizono[10ABCDEFG], Akinobu Taketomi[11ABCDEFG], Shuichi Matsumoto[12ABCDEFG], Tsutomu Tamai[13ABCDEFG], Toyokichi Muro[14ABCDEFG], Kazuhiko Nakao[15ABCDEFG], Kunitaka Fukuizumi[16ABCDEFG], Tatsuji Maeshiro[17ABCDEFG], Osami Inoue[18ABCDEFG], Michio Sata[2ABCDEFG]

[1] Clinical Research Center, National Nagasaki Medical Center, Omura City, Nagasaki, Japan
[2] Division of Gastroenterology, Department of Medicine, Kurume University School of Medicine, Kurume City, Fukuoka, Japan
[3] Department of Surgery, National Hospital Organization Kyushu Medical Center, Chuo-ku, Fukuoka City, Fukuoka, Japan
[4] 1st Department of Internal Medicine, Oita University Faculty of Medicine, Hasama-machi, Yufu City, Oita, Japan
[5] Department of Hepatology, Fukuoka Red Cross Hospital, Minami-ku, Fukuoka City, Fukuoka, Japan
[6] Department of Internal Medicine, Saga University Faculty of Medicine, Saga City, Saga, Japan
[7] Department of Gastroenterology and Hepatology, Graduate School of Medical Sciences, Kumamoto University, Kumamoto City, Kumamoto, Japan
[8] Department of Internal Medicine II, Miyazaki Medical College, Kiyotake-cho, Miyazaki-gun, Miyazaki, Japan
[9] 3rd Department of Internal Medicine, University of Occupational and Environmental Health, Kitakyusyu City, Fukuoka, Japan
[10] Department of Hepatology, Nanpuh Hospital, Kagoshima City, Kagoshima, Japan
[11] Department of Surgery and Science, Graduate school of medical sciences, Kyushu University, Fukuoka City, Fukuoka, Japan
[12] Department of Internal Medicine, Fukuoka Tokusyukai Medical Center, Kasuga City, Fukuoka, Japan
[13] Digestive Disease and Life-Style Related Disease, Health Research Human and Environmental Sciences, Kagoshima University, Kagoshima City, Kagoshima, Japan
[14] Department of Gastroenterology, National Hospital Organization Oita Medical Center, Oita City, Oita, Japan
[15] Department of Gastroenterology and Hepatology, Nagasaki University School of Medicine, Nagasaki City, Nagasaki, Japan
[16] Department of Gastroenterology, National Hospital Organization, Kyushu Medical Center, Fukuoka City, Fukuoka, Japan
[17] 1st Department of Internal Medicine, Faculty of Medicine, University of the Ryukyus, Nakagami-gun, Okinawa, Japan
[18] Department of Gastroenterology, Nagasaki Rousai Hospital, Sasebo City, Nagasaki, Japan

Source of support: Departmental sources

Summary

Background: The incidence of hepatocellular carcinoma (HCC) in Japan has still been increasing. The aim of the present study was to analyze the epidemiological trend of HCC in the western area of Japan, Kyushu.

Material/Methods: A total of 10,010 patients with HCC diagnosed between 1996 and 2008 in the Liver Cancer study group of Kyushu (LCSK), were recruited for this study. Cohorts of patients with HCC were categorized into five year intervals. The etiology of HCC was categorized to four groups as follows; B: HBsAg positive, HCV-RNA negative, C: HCV-RNA positive, HBsAg negative, B+C: both of HBsAg and HCV-RNA positive, non-BC: both of HBsAg and HCV-RNA negative.

Results: B was 14.8% (1,485 of 10,010), whereas 68.1% (6,819 of 10,010) had C, and 1.4% (140 of 10,010) had HCC associated with both viruses. The remaining 1,566 patients (15.6%) did not associate with both viruses. Cohorts of patients with HCC were divided into six-year intervals (1996–2001 and 2002–2007). The ratio of C cases decreased from 73.1% in 1996–2001 to 64.9% in 2002-2007. On the other hand, B and -nonBC cases increased significantly from 13.9% and 11.3% in 1996-2001 to 16.2% and 17.6% in 2002-2007, respectively.

Conclusions: The incidence of hepatocellular carcinoma associated with hepatitis C infection decreased after 2001 in Kyushu area. This change was due to the increase in the number and proportion of the HCC not only nonBC patients but also B patients.

key words: hepatitis virus • hepatocellular carcinoma • Japan

Full-text PDF: http://www.medscimonit.com/fulltxt.php?ICID=881375
Word count: 1778
Tables: 3
Figures: 2
References: 32

Author's address: Hiroshi Yatsuhashi, Clinical Research Center, National Nagasaki Medical Center, 2-1001-1 Kubara, Omura City, Nagasaki, Japan, e-mail: yatsuhashi@nmc.hosp.go.jp

Background

The three leading causes of death in Japan are malignancy neoplasms, cardiovascular diseases, and cerebrovascular diseases. Since 1981, malignant neoplasms have been the leading cause of death in Japan. For the last 30 years, liver cancer has been the third leading cause of death from malignant neoplasms in men. In women, liver cancer has ranked fifth during the past decade [1]. Hepatocellular carcinoma (HCC) accounts for 85% to 90% of primary liver cancers[2] and the age-adjusted HCC mortality rate has increased in recent decades in Japan [3]. Similarly, a trend of increasing rates of HCC has been reported from several developed countries in North America, Europe and Asia [4,5]. HCC often develops in patients with liver cirrhosis caused by hepatitis B virus (HBV), hepatitis C virus (HCV), excessive alcohol consumption, or nonalcoholic fatty liver disease. Of the hepatitis viruses which cause HCC, HCV is predominant in Japan [6–9].

Although the age-adjusted incidence of HCC has increased in Japan, sequential changes in etiology of HCC patients between 2001 and 2008 are not fully understood [10]. To clarify factors affecting epidemiological changes in Japanese HCC patients, especially the recent trend of HCC, we analyzed the epidemiological trend of HCC in the western area of Japan, Kyushu area.

Material and Methods

Patients

A total of 10,010 patients with HCC diagnosed between 1996 and 2008 in the Liver Cancer study group of Kyushu (LCSK), were recruited for this study. The diagnosis of HCC was based on AFP levels and imaging techniques including ultrasonography (USG), computerized tomography (CT), magnetic resonance imaging (MRI), hepatic angiography (HAG), and/or tumor biopsy. The diagnostic criteria for HCC were either a confirmative tumor biopsy or elevated AFP (>20 ng/mL) and neovascularization in HAG and/or CT.

Etiology of HCC

A diagnosis of chronic HCV infection was based on the presence of HCV-RNA detected by polymerase chain reaction (PCR), whereas diagnosis of chronic HBV infection was based on the presence of hepatitis B surface antigen (HBsAg). The etiology of HCC was categorized to four groups as follows; **B:** HBsAg positive, HCV-RNA negative, **C:** HCV-RNA positive, HBsAg negative, **B+C:** both of HBsAg and HCV-RNA positive, **nonBC:** both of HBsAg and HCV-RNA negative.

Statistical analysis

The data were analyzed by the Mann-Whitney test for the continuous ordinal data, the x2 test with Yates' correction and the Fisher exact test for the association between two qualitative variables. The standard deviation was calculated based on the binomial model for the response proportion. P<0.05 was considered statistically significant.

Results

Clinical features of the studied patients

A total of 10,010 patients with HCC were diagnosed at our study group from 1996 to 2008. Table 1 show that the proportion of patients diagnosed with B was 14.8% (1,485 of 10,010), whereas 68.1% (6,819 of 10,010) had C, and an additional 1.4% (140 of 10,010) had HCC associated with both viruses. The remaining 1,566 patients (15.6%) did not associate with both viruses. In analysis of patients in HCC by category, the median age of patients at diagnosis of B was 57 years old significant younger than other types HCC(**C: 69, nonBC: 70,.B+C 65 years old).**

As shown in Figures 1 and 2, the number and ratio of B cases remained unchanged from1996 to 2001 and thereafter increased and plateaued, whereas C rapidly increased from 1996 to 2000 and thereafter decreased and plateaued. In addition, the number and ratio of the **nonBC** cases has increased continued gradually and continued in this study period.

Change of etiology in patients with HCC during the period 1996–2007 with 6-years intervals

Cohorts of patients with HCC were divided into six-year intervals (1996–2001 and 2002–2007). Table 2 show that the incident rate of C decreased significantly from 73.1% in 1996-2001 to 64.9% in 2002-2007 (1996–2001 vs. 2002–2007, p=<0.001). On the other hand, the incident rate of B and **-nonBC** increased significantly from 13.9% and 11.3% in 1996-2001 to 16.2% and 17.6% in 2002-2007, respectively. Not only the incident rate but also number of B and **-nonBC** became larger in same 6 years periods.

Table 3 shows that male/female ratio of C and **-nonBC** decreased significantly from 2.2 and 4.0 in 1996-2001 to 1.8 and 2.7 in 2002-2007, respectively (p<0.001). The ratio became clearly smaller, indicates an increase in female patients with C and **nonBC.** On the other hand, the male/female ratio of B patients did not significantly change during the period. The median age at diagnosis of **B, C,** and **nonBC** in six-year intervals were significant increase from 56 to 58, from 67 to 71 and from 68 to 71 years of age during the period.

Discussion

Our study was the twenty-three major liver center-based study designed to examine the sequential change in the background of HCC patients during the past 13 years, 1996–2008. More than 80% of our patients had chronic HBV or HCV infections. During this observation period, the number and proportion of HCC-C reached a peak in 2000 and thereafter decreased and became stabilized. Previous studies from Japan reported that the proportion of the HCC patients with HCV infection had been increased and reached a plateau in the period of 1981–2001 [1,3,10–12]. However, in our study, the number and proportion of the HCC patients with HCV infection cases decreased in 2001–2008. The reason may be explained as follows; interferon therapy for chronic hepatitis C may have been associated with a decreased incidence of HCC [13–17]. Oral supplementation with a oral branched-chain amino acids has been useful in the prevention HCC [18]. Finally, the chronically HCV-infected

Table 1. The characteristic of HCC patients during the period of 1996–2008.

Age (y.o.)	B		C		nonB		B+C		Total
	Male	Female	Male	Female	Male	Female	Male	Female	
0–	1	0	0	1	0	0	0	0	2
10–	4	1	0	0	0	2	0	0	7
20–	6	2	1	0	1	1	0	0	11
30–	31	5	4	0	11	3	2	0	56
40–	204	22	130	12	32	15	12	0	427
50–	507	66	728	145	167	32	31	6	1,682
60–	287	118	1836	741	411	102	35	13	3,543
70–	140	64	1775	947	483	133	22	14	3,578
80–	9	18	271	214	97	65	1	4	679
90–	0	0	9	5	9	2	0	0	58
Total	1,189	296	4,754	2,065	1,211	355	103	37	10,010
	1,485 (4.8%)		6,819 (68.1%)		1,566 (15.6%)		140 (1.4%)		
Median	57	63	67	70	68	70	61	68	67
	57		69		70		65		
Mean	56	64	68	71	69	71	62	68	67
	58		68		68		63		
Range	1–87	14–89	27–94	0–93	28–96	17–90	36–82	55–82	0–96
	1–89		0–94		17–96		36–82		

Age: B vs. C p≤0.001; B vs. B+C p≤0.001; B vs. nonBC p≤0.001; C vs. BC p≤0.001; C vs. nonBC p=0.043; BC vs. nonB+C p≤0.001. IQR – interquartile range; SD – standard deviation.

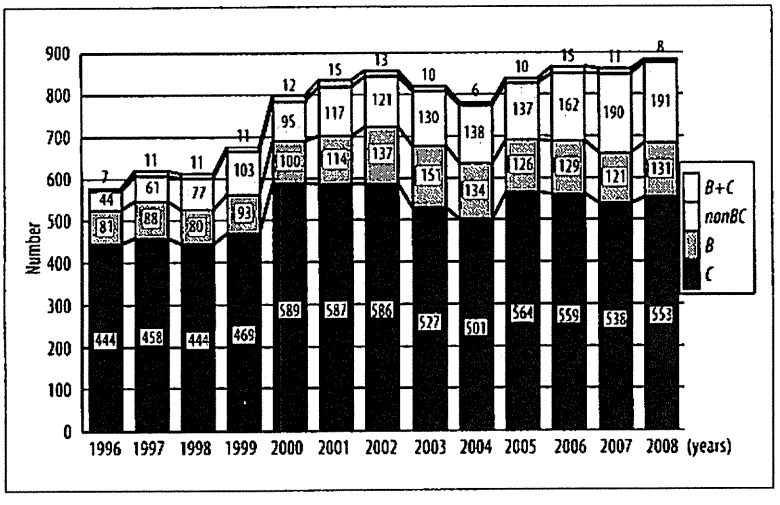

Figure 1. Sequential changes in the number of HCC patients categorized by etiology during the period 1996–2008.

population is aging in Japan. Yoshizawa et al. reported that age-specific prevalence for the presence of HCVAb among ~300,000 voluntary blood donors from Hiroshima in 1999 clearly increased with the age, reaching the highest proportion of 7% in individuals who were more than 70 years old [10,19]. In this study, the median age of the HCC patients with HCV infection steadily increased from 67 to 71 years of age during the studied period. In a word, HCV infected people become older with years in Japan and they were regarded as a high risk for HCC.

The prevalence rate of HBV in Kyushu area has been reported to be higher than other area in Japan [1]. In Kyushu area, 95% of patients with chronic HBV infection had HBV genotype C except for Okinawa [20]. HBV genotype C is thought to be associated with higher incidence of HCC

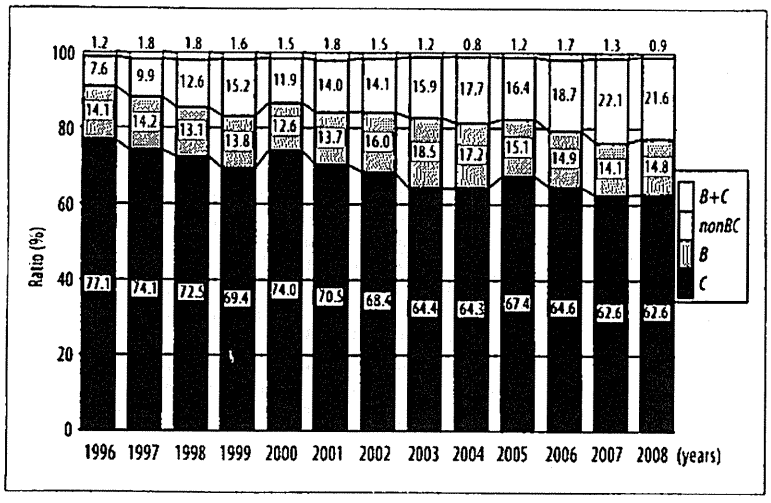

Figure 2. Sequential changes in the ratio of HCC patients categorized by etiology during the period 1996–2008.

Table 2. Change of etiology in patients with HCC during the period 1996–2007 with 6-years intervals.

Period		1996–2001	2002–2007	P value
Number		3,023	4,173	
Sex	Male	2,162	2,849	
	Female	861	1,324	
Ratio (male/female)		2.5	2.2	0.003
Age (y.o.) (IQR)		66 (14)	69 (12)	<0.001
Hepatitis virus (%)	B	13.9	16.2	
	C	73.1	64.9	
	B+C	1.7	1.3	
	nonBC	11.3	17.6	0.001

QR – interquartile range.

Table 3. The median age and male/female ratio of HCC patients during the period of 1996–2007.

Period		1996–2001	2002–2007	P value
B				
Age (y.o.) (IQR)		56 (14)	58 (15)	0.001
Sex	Male	331	519	
	Female	88	157	
Ratio (male/female)		3.8	3.3	0.391
C				
Age (y.o.) (IQR)		67 (9)	71 (11)	<0.001
Sex	Male	1,524	1,753	
	Female	687	955	
Ratio (male/female)		2.2	1.8	0.002
nonBC				
Age (y.o.) (IQR)		68 (12)	71 (13)	<0.001
Sex	Male	273	534	
	Female	69	201	
Ratio (male/female)		4.0	2.7	0.012

QR – interquartile range.

compared with other HBV genotypes [21]. In the present study, the incident rate of HCC patients with HBV infection became larger in this study period. To explain this change, we must consider from two viewpoints. The one is that the number of patients with HCC caused by HCV infection decreased, the other is that the proportion of chronic HBV infected patients who have reached the age of developing HCC is relatively high as described below.

Nationwide health survey for HBsAg in the over 40 years of age population had been done between 2002 and 2006 in Japan. This survey reports indicated that the average HBsAg prevalence was 1.2% in the total Japanese population patients with chronic HBV infection [10] and the age-specific prevalence of HBsAg was higher in the group aged between 50 (1.4%) and 55 years (1.5%). In the HCC patients with HBV genotype C, the mean age was 55 years in Japan [20]. This overlap between age-specific prevalence and hepatocellular carcinogenic age would be associated with the increase of HCC patients with HBV infection. Nucleoside analogue reverse transcriptase inhibitor (NARTI) therapy effectively reduces the incidence of HCC in chronic hepatitis B patients [22,23]. However, Interferon therapy for chronic hepatitis C started from 1992, whereas NARTI therapy for HBV started from 2000 in Japan [24,25]. Hence, HBV associated HCC will probably decrease in Japan during the next 10 to 20 years.

The survey of HCC patients associated with nonBC infection in Japan was conducted by Inuyama Hepatitis Research Group from 1995 to 2003. The ratio of HCC patients with nonBC accounted 9.3% [1]. In the present study, the ratio of HCC patients with nonBC was 14.1%. Furthermore, the number and the proportion of HCC patients with nonBC have been gradually increasing in the periods. The current two studies account for the increase in number and proportion of HCC patients with nonBC. First, Lai et al. reported

that type 2 diabetes increases the risk of developing HCC in those who are HCV negative or have a high level of total cholesterol [26]. Second, Nakano et al. reported that epidemiological studies on diabetes mellitus revealed that the number of patients with diabetes mellitus is gradually increasing in Japan along with development of car society and westernization of food intake. Since prevalence of diabetes mellitus increases with aging, proportion of individuals with diabetes mellitus aged over 60 has exceeded two-third of estimated total number of patients (7.40 million in 2002) in Japan where aging of society is rapidly progressing [27]. In a word, the number of type 2 diabetes people is increasing in Japan and they were regarded as a high risk for HCC. Then, the number and the proportion of HCC patients with nonBC have been increased recent twelve years in Japan.

It is known that 2 to 4 decades of chronic HCV infection are required to develop cirrhosis and subsequent HCC [28–31]. The number of HCC cases has increased in Japan, because individuals infected with HCV during the past have grown old and have reached the cancer-bearing age. The prevalence of HCV infection in young Japanese individuals is low and the incidence of HCVAb is very low because of preventative actions against HCV infection such as the screening of blood products for HCV and the use of sterile medical equipment [32]. Additionally, we showed that the number and proportion of patients with HCC-C cases decreased, whereas the number and ratio of HCC-nonBC steadily increased during the studied period. These findings may be expected that the incidence of HCC patients with nonBC in Japan may continue to increase even after the consequence of the HCV epidemic level off, a country that is far advanced with regard to HCC patients with HCV infection, in the near future.

Conclusions

In summary, HCC patients had increased from 1996 to 2000 and this increase was originated from HCC patients with HCV infection. The number and proportion of HCC patients with HCV infection reached a peak in 2000 and thereafter decreased and became stabilized. The incidence of hepatocellular carcinoma associated with hepatitis C infection decreased after 2001 in Kyushu area. This change was due to the increase in the number and proportion of the HCC not only nonBC patients but also B patients.

References:

1. Umemura T, Kiyosawa K: Epidemiology of hepatocellular carcinoma in Japan. Hepatol Res, 2007; 37(Suppl.2): S95–100
2. El-Serag HB, Rudolph KL: Hepatocellular carcinoma: epidemiology and molecular carcinogenesis. Gastroenterology, 2007; 132: 2557–76
3. Kiyosawa K, Tanaka E: Characteristics of hepatocellular carcinoma in Japan. Oncology, 2002; 62: 5–7
4. McGlynn KA, Tsao L, Hsing AW et al: International trends and patterns of primary liver cancer. Int J Cancer, 2001; 94: 290–96
5. Bosch FX, Ribes J, Diaz M, Cleries R: Primary liver cancer: worldwide incidence and trends. Gastroenterology, 2004; 127: S5–16
6. Hamasaki K, Nakata K, Tsutsumi T et al: Changes in the prevalence of hepatitis B and C infection in patients with hepatocellular carcinoma in the Nagasaki Prefecture, Japan. J Med Virol, 1993; 40: 146–49
7. Kato Y, Nakata K, Omagari K et al: Risk of hepatocellular carcinoma in patients with cirrhosis in Japan. Analysis of infectious hepatitis viruses. Cancer, 1994; 74: 2234–38
8. Shiratori Y, Shiina S, Imamura M et al: Characteristic difference of hepatocellular carcinoma between hepatitis B- and C-viral infection in Japan. Hepatology, 1995; 22: 1027–33
9. Shiratori Y, Shiina S, Zhang PY et al: Does dual infection by hepatitis B and C viruses play an important role in the pathogenesis of hepatocellular carcinoma in Japan? Cancer, 1997; 80: 2060–67
10. Kiyosawa K, Umemura T, Ichijo T et al: Hepatocellular carcinoma: recent trends in Japan. Gastroenterology, 2004; 127: S17–26
11. Taura N, Yatsuhashi H, Hamasaki K et al: Increasing hepatitis C virus-associated hepatocellular carcinoma mortality and aging: Long term trends in Japan. Hepatol Res, 2006; 34: 130–34
12. Taura N, Hamasaki K, Nakao K et al: Aging of patients with hepatitis C virus-associated hepatocellular carcinoma: long-term trends in Japan. Oncol Rep, 2006; 16: 837–43
13. Nishiguchi S, Kuroki T, Nakatani S et al: Randomised trial of effects of interferon-alpha on incidence of hepatocellular carcinoma in chronic active hepatitis C with cirrhosis. Lancet, 1995; 346: 1051–55
14. Nishiguchi S, Shiomi S, Nakatani S et al: Prevention of hepatocellular carcinoma in patients with chronic active hepatitis C and cirrhosis. Lancet, 2001; 357: 196–97
15. Kasahara A, Hayashi N, Mochizuki K et al: Risk factors for hepatocellular carcinoma and its incidence after interferon treatment in patients with chronic hepatitis C. Osaka Liver Disease Study Group. Hepatology, 1998; 27: 1394–402
16. Ikeda K, Saitoh S, Arase Y et al: Effect of interferon therapy on hepatocellular carcinogenesis in patients with chronic hepatitis type C: A long-term observation study of 1,643 patients using statistical bias correction with proportional hazard analysis. Hepatology, 1999; 29: 1124–30
17. Makiyama A, Itoh Y, Kasahara A et al: Characteristics of patients with chronic hepatitis C who develop hepatocellular carcinoma after a sustained response to interferon therapy. Cancer, 2004; 101: 1616–22
18. Muto Y, Sato S, Watanabe A et al: Effects of oral branched-chain amino acid granules on event-free survival in patients with liver cirrhosis. Clin Gastroenterol Hepatol, 2005; 3: 705–13
19. Yoshizawa H: Hepatocellular carcinoma associated with hepatitis C virus infection in Japan: projection to other countries in the foreseeable future. Oncology, 2002; 62: 8–17
20. Orito E, Mizokami M: Hepatitis B virus genotypes and hepatocellular carcinoma in Japan. Intervirology, 2003; 46: 408–12
21. Orito E, Mizokami M: Differences of HBV genotypes and hepatocellular carcinoma in Asian countries. Hepatol Res, 2007; 37: S33–35
22. Matsumoto A, Tanaka E, Rokuhara A et al: Efficacy of lamivudine for preventing hepatocellular carcinoma in chronic. Hepatol Res, 2005; 32(3): 173–84
23. Xu J, Shi J, Wang YP et al: Milder liver cirrhosis and loss of serum HBeAg do not imply lower risk for. Med Sci Monit, 2009; 15(6): CR274–79
24. Hayashi N, Takehara T: Antiviral therapy for chronic hepatitis C: past, present, and future. J Gastroenterol, 2006; 41(1): 17–27
25. Kumashiro R, Kuwahara R, Ide T et al: Subclones of drug-resistant hepatitis B virus mutants and the outcome of breakthrough hepatitis in patients treated with lamivudine. Intervirology, 2003; 46(6): 350–54
26. Lai MS, Hsieh MS, Chiu YH, Chen TH: Type 2 diabetes and hepatocellular carcinoma: A cohort study in high prevalence area of hepatitis virus infection. Hepatology, 2006; 43: 1295–302
27. Nakano T, Ito H: Epidemiology of diabetes mellitus in old age in Japan. Diabetes Res Clin Pract, 2007; 77(Suppl.1): S76–81
28. Deuffic S, Poynard T, Valleron AJ: Correlation between hepatitis C virus prevalence and hepatocellular carcinoma mortality in Europe. J Viral Hepat, 1999; 6: 411–13
29. El-Serag HB, Mason AC: Rising incidence of hepatocellular carcinoma in the United States. N Engl J Med, 1999; 340: 745–50
30. Planas R, Balleste B, Antonio Alvarez M et al: Natural history of decompensated hepatitis C virus-related cirrhosis. A study of 200 patients. J Hepatol, 2004; 40: 823–30
31. Davila JA, Morgan RO, Shaib Y et al: Hepatitis C infection and the increasing incidence of hepatocellular carcinoma: a population-based study. Gastroenterology, 2004; 127: 1372–80
32. Sasaki F, Tanaka J, Moriya T et al: Very low incidence rates of community-acquired hepatitis C virus infection in company employees, long-term inpatients, and blood donors in Japan. J Epidemiol, 1996; 6: 198–203

J Gastroenterol (2011) 46:92–100
DOI 10.1007/s00535-010-0293-6

ORIGINAL ARTICLE—LIVER, PANCREAS, AND BILIARY TRACT

Alpha-fetoprotein above normal levels as a risk factor for the development of hepatocellular carcinoma in patients infected with hepatitis C virus

Masakuni Tateyama · Hiroshi Yatsuhashi · Naota Taura · Yasuhide Motoyoshi · Shinya Nagaoka · Kenji Yanagi · Seigo Abiru · Koji Yano · Atsumasa Komori · Kiyoshi Migita · Minoru Nakamura · Hiroyasu Nagahama · Yutaka Sasaki · Yuzo Miyakawa · Hiromi Ishibashi

Received: 4 August 2009 / Accepted: 6 July 2010 / Published online: 14 August 2010

Abstract
Background Noninvasive risk factors are required for predicting the development of hepatocellular carcinoma (HCC) not only in patients with cirrhosis but also in those with chronic hepatitis who are infected with hepatitis C virus (HCV).
Methods A total of 707 patients with chronic HCV infection without other risks were evaluated for the predictive value of noninvasive risk factors for HCC, including age, sex, viral load, genotype, fibrosis stage, aspartate and alanine aminotransferase levels, bilirubin, albumin, platelet count, and alpha-fetoprotein (AFP) at entry to the study, as well as interferon (IFN) therapy they received.
Results The ten-year cumulative incidence rates of HCC for patients with fibrosis stages F0/F1, F2, F3, and F4 were 2.5, 12.8, 19.3, and 55.9%, respectively. Multivariate analysis identified age ≥57 years [hazard ratio (HR) 2.026, $P = 0.004$], fibrosis stage F4 (HR 3.957, $P < 0.001$), and AFP 6–20 ng/mL (HR 1.942, $P = 0.030$) and ≥20 ng/mL (HR 3.884, $P < 0.001$), as well as the response to IFN [relative risk (RR) 0.099, $P < 0.001$], as independent risk factors for the development of HCC. The ten-year cumulative incidence rates of HCC in the patients with AFP levels of <6, 6–20, and ≥20 ng/mL at entry were 6.0, 24.6, and 47.3%, respectively.
Conclusions Not only high (>20 ng/mL), but also even slightly elevated (6–20 ng/mL) AFP levels, could serve as a risk factor for HCC to complement the fibrosis stage. In contrast, AFP levels <6 ng/mL indicate a low risk of HCC development in patients infected with HCV, irrespective of the fibrosis stage.

Keywords Alpha-fetoprotein · Hepatitis C virus · Hepatocellular carcinoma

Introduction

Worldwide, an estimated 170 million people are persistently infected with hepatitis C virus (HCV) [1, 2], and they are at high risk of developing hepatocellular carcinoma (HCC) [1, 3–5]. Several factors have been identified that increase the risk of HCC, including, age, male gender, and alcohol intake, as well as cirrhosis and the duration of infection [3, 5]. Of these factors, the stage of liver fibrosis parallels the risk for HCV-associated HCC. The annual incidence of HCC in patients with HCV-related cirrhosis ranges from 1 to 7% [6, 7]. Although liver biopsy is the gold standard for the assessment of hepatic fibrosis [8, 9], it is too invasive a procedure to be acceptable as a routine test [10, 11]. In place of liver biopsy, the platelet count is used to estimate the degree of fibrosis [12–14], and low platelet counts have been shown to be a risk factor for the development of HCC in cirrhotic patients [13, 15, 16]. In this study, we tried to identify noninvasive markers for predicting the development of HCC in a large cohort of

M. Tateyama · H. Yatsuhashi (✉) · N. Taura · Y. Motoyoshi · S. Nagaoka · K. Yanagi · S. Abiru · K. Yano · A. Komori · K. Migita · M. Nakamura · H. Ishibashi
Clinical Research Center, National Nagasaki Medical Center, Nagasaki 856-8562, Japan
e-mail: yatsuhashi@nmc.hosp.go.jp

M. Tateyama · H. Nagahama · Y. Sasaki
Department of Gastroenterology and Hepatology, Graduate School of Medical Sciences, Kumamoto University, Kumamoto 860-8556, Japan

Y. Miyakawa
Miyakawa Memorial Research Foundation, Tokyo 107-0062, Japan

patients with chronic HCV infection during a long observation period.

Patients and methods

Study design

Between January 1992 and December 2003, 832 patients were identified who were positive for both anti-HCV, by a second or third-generation enzyme-linked immunosorbent assay (ELISA), and for HCV RNA by polymerase chain reaction (PCR). These patients underwent liver biopsy guided by ultrasonography (US) at the National Nagasaki Medical Center. Of the 832 patients, 125 (15.0%) were excluded according to the following criteria: (1) positive for hepatitis B surface antigen (HBsAg) ($n = 12$); (2) heavy habitual drinking defined as an average daily consumption of >100 g ethanol ($n = 26$); (3) presence of autoimmune hepatitis (AIH), primary biliary cirrhosis, or idiopathic portal hypertension ($n = 8$); (4) positive antinuclear antibody (defined as a titer of >320×) without a diagnosis of AIH ($n = 8$); or (5) a short follow-up period (<180 days) ($n = 71$). The remaining 707 patients were analyzed retrospectively for the incidence of HCC. Their medical histories had been recorded, with the results of routine tests for blood cell counts, liver biochemical parameters, and markers for HCV infection at the time of US-guided liver biopsy at regular intervals. Complete blood cell counts and biochemical tests were performed, using automated procedures, at the clinical pathology laboratories of the National Nagasaki Medical Center. Iinformed consent was obtained from each patient included in the study, and the study protocol conformed to the ethical guidelines of the 1975 Declaration of Helsinki as reflected in a-priori approval by the institution's human research committee.

Staging of hepatic fibrosis

Liver biopsy was taken by fine-needle aspiration (18G or 16G sonopsy) guided by US. Liver tissue specimens were fixed in 10% formalin, embedded in paraffin, and stained with hematoxylin and eosin. They were evaluated for the stage of hepatic fibrosis by a pathologist according to the criteria of Desmet et al. [17].

HCV RNA, HCV core antigen, and HCV genotypes

HCV RNA was determined by reverse transcriptase (RT)-PCR using a commercial kit (Amplicor HCV; Roche Diagnostic Systems, Basel, Switzerland). HCV core antigen was determined using the lumispot EIKEN HCV antigen assay (Eiken Chemicals, Tokyo, Japan). HCV core antigen levels were classified as low or high with the cutoff at 1,000 fmol/L [18, 19]. Genotypes of HCV were determined by RT-PCR with genotype-specific primers (HCV RNA core genotype; Roche Diagnostics, Tokyo, Japan) [20, 21].

Interferon therapy

During the observation period, 373 of the 707 (52.8%) patients received interferon (IFN) monotherapy, pegylated (PEG)-IFN monotherapy, combination therapy with IFN and ribavirin, or PEG-IFN and ribavirin. Sustained virological response (SVR) was defined as the absence of detectable HCV RNA by the end of treatment that persisted for longer than 6 months thereafter, while failure in meeting these criteria was judged as non-SVR. There was no relapse of viremia after 6 months among SVR patients.

Diagnosis of hepatocellular carcinoma

Patients were followed up with hematological and biochemical tests at intervals of 1–12 months. Liver imaging was performed by US at 6- to 12-month intervals in most patients at fibrosis stages F0–F2, while computed tomography (CT), magnetic resonance imaging (MRI), or US was performed at 3- to 6-month intervals in patients at fibrosis stages F3 and F4. HCC was diagnosed by typical vascular patterns on CT, MRI, or angiography, or by fine-needle biopsy of space-occupying lesions detected in the liver.

Statistical analysis

Continuous variables [platelet counts, albumin, total bilirubin, aspartate aminotransferase (AST), alanine aminotransferase (ALT), alpha-fetoprotein (AFP), HCV core antigen] were dichotomized with respect to the median value or clinically meaningful values in a multivariate analysis. To estimate the cumulative risk of developing HCC, the Kaplan–Meier method and the log-rank test were used. Cox proportional hazards regression analysis was performed to evaluate risk factors for HCC. Analysis was performed by Bonferroni's correction and data analysis was performed with SPSS ver. 11.0 (SPSS, Chicago, IL, USA).

Results

Characteristics at enrollment

Table 1 lists the characteristics of the 707 patients at enrollment. The median age was 57.0 years; 120 (17.0%)

Table 1 Demographic, clinical, and virological characteristics of 707 patients persistently infected with hepatitis C virus (HCV)

Age (years)	57.0 (19–79)
Male	351 (49.6%)
Observation period (years)	8.2 ± 4.4[a]
Interferon therapy	373 (52.8%)
Habitual alcohol intake	135 (19.1%)
Fibrosis stage	
F0/F1	273 (38.6%)
F2	193 (27.3%)
F3	121 (17.1%)
F4	120 (17.0%)
Platelet count ($\times 10^3/mm^3$)	156 (30–391)
Albumin (g/dL)	4.2 (2.7–5.3)
Total bilirubin (mg/dL)	0.7 (0.1–2.5)
Aspartate aminotransferase (AST; IU/L)	53 (11–422)
Alanine aminotransferase (ALT; IU/L)	82 (1–1,057)
Alpha-fetoprotein (AFP; ng/mL)	6 (1–510)
HCV core antigen	
≥1,000 fmol/L	539 (76.2%)
HCV genotype	
1b	510 (72.1%)
2a/2b	195 (27.6%)
Unknown	2 (0.3%)

Values are medians with ranges in parentheses, or means with SD in parentheses

[a] Mean ± SD

patients were diagnosed histologically with liver cirrhosis (fibrosis stage: F4) and the remaining 587 had chronic hepatitis (fibrosis stage F0, F1, F2, or F3). The median value of AFP was 6 ng/mL. The average follow-up period was 8.2 years. The patients were classified into three categories by the level of AFP; 350 patients (49.5%) had AFP levels of <6 ng/mL, 254 (35.9%) had levels between 6 and 20 ng/mL, and the remaining 103 (14.6%) had levels of ≥20 ng/mL.

IFN therapy and IFN response

Of the 120 patients with cirrhosis (fibrosis stage F4), 46 (38.3%) received IFN while the remaining 74 (61.7%) did not. The proportions of IFN-treated patients showing an SVR were 40.8% (56/137) in patients with F1; 37.6% (44/117) in those with F2; 32.8% (24/73) in those with F3; and 32.6% (15/46) in those with F4.

Risk factors for HCC

Cox regression analysis was performed on several variables, including age, sex, alcohol consumption, IFN therapy during the observation period, and biochemical as well as virological parameters. The following factors were identified as showing an increased risk for HCC by the univariate analysis: age; IFN therapy; fibrosis stage; platelet count; albumin; AST, ALT, and AFP levels; and HCV genotype (Table 2). Multivariate analysis was performed on these factors (Table 3), and the following were identified as independent risk factors: fibrosis stage (F4), AFP (6–20 and ≥20 ng/mL), age (≥57 years), and IFN therapy (SVR).

Development of HCC

During the follow-up period, HCC developed in 110 (15.6%) patients. Of the 110 patients with HCC, 58 (52.7%) were diagnosed with the disease by histological examination of biopsy-obtained or resected liver specimens. Of these 58 patients, 24 (41.3%) had hypovascular HCC.

Among the patients with HCC, only eight (7.2%) had AFP <6 ng/mL at the time of diagnosis of HCC. Figure 1 shows Kaplan–Meier estimates of the cumulative risk of HCC with respect to fibrosis stage at entry. The 10-year cumulative incidence rates of HCC for stages F0/F1, F2, F3, and F4 were 2.5, 12.8, 19.3, and 55.9%, respectively.

There were significant differences in cumulative incidence rates among the three groups of patients with different AFP levels. The 10-year cumulative risk of HCC was 6.0% in the 350 patients with AFP <6 ng/mL at the study entry, 24.6% in the 254 patients with AFP 6–20 ng/mL, and 47.3% in the 103 patients with AFP ≥20 ng/mL ($P < 0.001$) (Fig. 2). Of the 350 patients with AFP <6 ng/mL, 21 eventually developed HCC during the observation period. Fourteen of these 21 patients were ≥57 years old and 10 had fibrosis stage F3 or F4. In remarkable contrast, HCC ultimately developed in 84.5% of the patients with AFP ≥20 ng/mL.

The 10-year cumulative incidence rates of HCC were 3.1% in patients with SVR to IFN, 14.6% in patients with non-SVR, and 29.5% in the patients without IFN therapy (Fig. 3). Of the 139 patients with SVR, three (2.2%) eventually developed HCC during the observation period. These three patients had advanced fibrosis stages at the study entry (1 with F3 and 2 with F4). Figure 4 shows the cumulative incidence of HCC in the patients with different AFP levels, stratified by the fibrosis stage. In the patients with fibrosis stage F4, there were significant differences in HCC incidence between those with AFP levels of <6 and those with levels of ≥20 ng/mL.

Figure 5 shows the proportions of patients with different AFP levels stratified by the fibrosis stage. The proportion of patients with AFP <6 ng/mL decreased with the advance of fibrosis stage, and conversely, the proportion of patients with AFP ≥20 ng/mL increased with the advance of fibrosis stage. There was a strong correlation between AFP levels and the fibrosis stage.